TAMPEREEN TEKNILLINEN YLIOPISTO
TAMPERE UNIVERSITY OF TECHNOLOGY

VILLE ERLING

IMPLEMENTATION OF INTERIOR PERMANENT MAGNET SYNCHRONOUS MACHINES AND CONTROL IN A WIND POWER EMULATING TEST BENCH

Master of Science thesis

Supervisors: Ph.D. Jenni Rekola
Assist. Prof. Paavo Rasilo

TIIVISTELMÄ

TAMPEREEN TEKNILLINEN YLIOPISTO
Automaatiotekniikka
Erling, Ville: Avonapaisten kestomagneettitahtikoneiden ja säädön toteutus tuulivoimaa emuloivassa testipenkissä
Diplomityö, 58 sivua, 7 liitesivua
Marraskuu 2017
Pääaine: Tehoelektroniikka
Tarkastajat: Ph.D. Jenni Rekola, Assist. Prof. Paavo Rasilo
Avainsanat: Boombox, emuloiva testipenkki, tuulivoima, vektorisäätö

Kasvava huoli ilmastonmuutoksesta on aiheuttanut sen, että yritykset ja valtiot investoivat entistä enemmän uusiutuviin energiamuotoihin, jotka ovat vähemmän saastuttavia maapallolle. Tuulivoima on yksi niistä, ja sen suosio onkin kasvanut koko kaksituhattaluvun, mikä on aiheuttanut taloudellisen mielenkiinnon siihen, että tuulivoimaturbiineissa käytettävät generaattorit olisivat mahdollisimman tehokkaita.

Tämä diplomityö keskittyy tuulivoimaa emuloivaan testipenkkiin, jossa käytetään kestomagneettitahtikoneita. Testipenkki sijaitsee Tampereen teknillisellä yliopistolla tehoelektroniikan laboratoriossa, johon on asennettu moottori ja generaattori, joita ohjataan taajuusmuuttajilla. Moottori toimii voimalaitteena, jolle asetetaan jokin tietty momentti, joka emuloi tuulen nopeuden tuottamaa momenttia. Generaattorin puolelle tehdään oma ohjaus ja nämä koneet kytketään yhteen, jolloin niiden välissä on momenttianturi. Generaattoripuolen jännitteet ja virrat on mitattu Boombox sensoreilla ja sähkön laatua parannetaan LCL-suotimilla.

Testipenkkiä käytetään tutkimuskäytössä sen jälkeen, kun se on valmis. Mielenkiinnon kohteena on säätöjärjestelmän dynamiikka. Toinen mielenkiinnon kohde on staattorikäämien numeerinen mallinnus, jonka apuna käytetään koneisiin esiasennettuja mittakäämejä.

Testipenkki käyttää avonapaisia kestomagneettitahtimoottoreita, joissa induktanssit ovat eri pitkittäis- ja poikittais-akseleilla. Koneiden akselitehoiksi valittiin 17 kW. Molempien koneiden nimellispyörimisnopeus on 127 rpm. Koneiden sisään asennettiin myös inkrementaaliset enkooderit tarkempaan pyörimisnopeuden mittaukseen.

Testipenkki käyttää neljää taajuusmuuttajaa 61 A maksimivirralla. Taajuusmuuttajien diodisillat ohitettiin asentamalla sekä moottorin että generaattorin puolella taajuusmuuttajien DC-linkit yhteen, jolloin varmistettiin se, että teho on kaksisuuntaista. Generaattorin puolella oli myös VaconBus-adapterit, joilla mahdollistetaan itse luodun säädön käyttäminen.

Kestomagneettitahtigeneraattorin simulointimalli luotiin käyttäen dynaamisia yhtälöitä MATLAB:in Simulinkillä. Moottorin toiminta varmistettiin testaamalla sitä ilman kuormaa, minkä tulokset mitattiin ja dokumentoitiin.

ABSTRACT

TAMPERE UNIVERSITY OF TECHNOLOGY
Automation technology
Erling, Ville: Implementation of permanent magnet synchronous machines and control in a wind power emulating test bench
Master of Science thesis, 58 pages, 7 appendix pages
November 2017
Major: Power electronics
Supervisors: Ph.D. Jenni Rekola, Assist. Prof. Paavo Rasilo
Key words: Boombox, emulating test bench, vector control, wind power

The growing concern about climate change has effected to that the corporations and governments invest more and more to renewable energy sources, which are less pollutant to the atmosphere. One of the renewable energy sources is wind power and in whole this millennium the popularity of wind power has steadily risen, which has caused an economical interest to develop as efficient wind turbine generators as possible.

This thesis focuses on a wind power related test bench, in which permanent magnet synchronous machines are used. The test bench will be located in the laboratory of power electronics of Tampere University of Technology and it will have one motor and one generator, which are controlled by converters. The motor works as prime mover and it has an input of torque reference, which emulates the torque caused by the wind speed. Our own control is implemented on the generator side and between these two machines is installed a torque transducer. The voltages and the currents are measured by Boombox sensors and the power quality is enhanced by LCL filters.

The test bench will be used for research purposes after it is complete. Interest is to investigate the dynamics of the control system. The other interest is to model numerically the stator windings by the help of preinstalled measurement windings.

The test bench uses interior permanent magnet synchronous machines, where the inductances are different at direct- and quadrature-axes. The motor and generator were chosen with shaft powers of 17 kW. The nominal rotating speed in both was 127 rpm. Inside the machines were installed incremental encoders to provide more accurate measurement of the rotating speed.

Four commercial converters were chosen with 61 A maximum current. The diode bridges were bypassed for enabling bidirectional power flow, when connecting the DC-link together by two similar converters in motor and generator side. The generator side had also VaconBus adapters, which allow to develop our own control algorithms.

The MATLAB Simulink models of the permanent magnet synchronous generator were created based on the dynamic equations, which were then simulated. The motor operation was verified by testing it without load, and the results were measured and documented.

PREFACE

My thesis was done in the Faculty of Computing and Electrical Engineering at Tampere University of Technology, where my supervisor was Ph.D. Jenni Rekola and examiner was Assist. Prof. Paavo Rasilo. The thesis was a part of wind power emulating test bench, which was implemented in the laboratory of power electronics.
I want to thank my supervisor, examiner, family and friends who supported me. I want to thank also the people in TUT Lab and personnel in the laboratory, who helped and gave me advices.

Ville Erling
Tampere, 13.10.2017

CONTENTS

LIST OF ABBREVIATIONS AND NOTATIONS

Symbols:

α	Fortescue operator ($1\angle 120°$)
A	Area (m^2)
B	Friction coefficient
C	Capacitance (F) or capacitor
c	Utility coefficient
δ	Angle between stationary and synchronous reference frame
f	Frequency (Hz)
γ	Stator current angle (°)
G	Transfer function
I	Current (A)
J	Inertia (kgm^2)
K	Gain
λ	Tip speed ratio
L	Inductance (H) or inductor
m	Modulation index
n	Speed (RPM)
Ψ	Flux linkage (Wb)
P	Power (W)
p	The amount of pole pairs
ρ	Density (kg/m^3)
R	Resistance (Ω)
r	Length of the blade (m)
s	Laplace variable
θ	Space vector angle or blade angle
T	Torque (Nm) or period (1/s)
$\vec{v}$	Space vector
v	Instantaneous value of the voltage or speed (m/s)
V	Voltage (V)
ω	Angular velocity (rad/s)
ζ	Damping factor
Z	Impedance (Ω)

Abbreviations:

AC	Alternating current
AFE	Active front end
AlNiCo	Aluminum-nickel-cobalt
ASIC	Application specific integrated circuit
DC	Direct current
DFIG	Double-fed induction machine
DTC	Direct torque control
DUI	Datum universal interface
FOC	Field oriented control
FRT	Fault ride through
HIL	Hardware in the loop
IGBT	Insulated gate bipolar transistor
IM	Induction machine
IPMSM	Interior permanent magnet synchronous machine
LVRT	Low voltage ride through
MPPT	Maximum power point tracking
MTPA	Maximum torque per ampere
NdFeB	Neodymium-iron-boron
PLL	Phase-locked loop
PMSG	Permanent magnet synchronous generator
PMSM	Permanent magnet synchronous machine
ppr	Pulses per revolution
PWM	Pulse width modulation
RMS	Root mean square
SM	Synchronous machine
SmCo	Samarium-cobalt
SPWM	Sinusoidal pulse width modulation

Subscripts:

α	Real component of stationary reference frame
a	Phase a or amplitude
β	Imaginary component of stationary reference frame
b	Phase b
c	Phase c or carrier or converter
d	Real component of synchronous reference frame or damping
dc	Direct current
Δ	Delta connection
e	Electrical
f	Frequency or filter
fund	Fundamental
g	Grid
i	Integrate
L	Load
LC	Inductive and capacitive
m	Magnetizing or modulating
mec	Mechanical
n	Nominal
p	Proportional or used in utility coefficient
pm	Permanent magnet
q	Imaginary component of synchronous reference frame
res	Resonant
RMS	Root mean square
s	Stator
sm	Stator maximum
sl	Stator leakage
w	Wind
Y	Star connection

1 INTRODUCTION

The average temperature of earth has steadily grown since 1960 and in the same time the concentration of the carbon dioxide in the atmosphere has risen. This phenomenon is widely discussed and it is known as the climate change. It is caused by a phenomenon known as the greenhouse effect, which means that most of the heat radiation coming from the sun to earth, does not reflect back to space. The greenhouse effect is vital to people in earth, but increased amount carbon dioxide and other greenhouse gases intensify it. This causes multiple problems, like rise of the sea level, the melting of the glaciers, dryness and extreme weather conditions all over the earth. The climate change cannot be stopped, but its effect can be reduced. The biggest sources of carbon dioxide are fossil fuels, which come from energy production, industry and traffic. The best way to reduce the effect of climate change is to remove or reduce the use of them. For example it can be done by replacing them in energy production by renewable energy sources or using vehicles with less emissions in traffic. On the other hand forests and flora bind carbon dioxide. By planting new forests, which are known as carbon sinks, can the amount of carbon dioxide be reduced in the atmosphere and prevent the climate change. [1]

Preventing the climate change is not an easy task, because it requires collaboration between countries, policies, regulations, technology and common will to commit to the appointed goals, which were decided last time in Paris in December 2015 and known as the Paris Agreement. Its main goal was to keep the rise of average level of global temperature under two Celsius degrees compared to pre-industrial level within this century [2]. Growing concern about climate change for decades, limited raw-material resources and oil crisis back in the 1970 established a fertile land for the development of the renewable energy sources [3]. There are several renewable energy sources based on where the energy come from, which are solar, wind, water, bio and geothermal. Especially wind power development and installations have increased. It has been affected by the fact that wind is distributed steadily all over the world and the windiest places are the coasts of the seas. The size of rotor diameter in wind turbines at the 80s was approximately 20 meters compared to the wind turbines nowadays, in which the size of the rotor diameter can be up to 130 meters.

There has been significant effort put on wind power in whole area of the European Union since year 2000. In that time the installed capacity of the wind power was 12.9 GW and 15 years later in 2015 the capacity was 141.6 GW. The investments to wind power have risen every year, which is ensured the steady growth. In 2015 the biggest money spender was the United Kingdom (€12.5 billion), because of the construction of the wind farms. In the same year the biggest wind power capacity installer was Germany

(6 GW), which consisted almost half of the whole EU. In 2015 wind power produces 11.4% of the annual electricity consumption in the EU. Investing to wind power requires, besides investments, also good regulations, policies and believe for future wind power projects by the governments of the countries. [4]

The installed capacity to wind power increases every year. Therefore, the requirement set for the operation of the wind turbines during the grid faults are nowadays more strict. Traditional generators used in wind turbines are doubly-fed induction generators (DFIG) and permanent magnet synchronous generators. Both generator types have pros and cons. This thesis objective is to document and implement a test bench, which emulates wind turbine generator by using a permanent magnet synchronous generator and the turbine is emulated by a permanent magnet synchronous motor.

The test bench works as real time hardware in the loop (HIL) simulation environment including commercial power converters, whose control algorithms are bypassed and replaced by self-created control algorithms. The control signals are transferred from MATLAB Simulink to the driver circuit of the power converters by using Boombox. The thesis will feature construction, modeling, simulating, controlling and testing the permanent magnet synchronous machines. After construction is complete, the test bench will be used for research purposes, where the focus is to investigate the dynamics of the control system.

The thesis is organized into chapters, the structure and operation principle of PMSG is presented in Chapter 2. Chapter 2 describes also the fundamentals of space vector theory and dynamic modeling of the PMSM.

A description of the developed laboratory setup is presented in Chapter 3. It consists of installation of the machines, converter, filters and measurements.

Chapter 4 consists of simulation results, which was done by Simulink. It ends to testing the real motor to verify the operation without load.

Finally, Chapter 5 draws the conclusion. It consists of reviewing the results and the future work.

2 FUNDAMENTALS OF PERMANENT MAGNET WIND TURBINE GENERATORS

Electric machines nowadays can be found almost everywhere. They are used for different applications such as pumps, vehicles, power tools, fans etc. There are multiple ways to choose the right electric machine for specific application, which can be based on the drive cycles, operating environment or other parameters used in application. The most common types of electric machines are synchronous machine (SM), induction machine (IM) and DC-machine. The electric machine is essential for industry, because 65% of the consumed electricity is used by electric machines [5]. In power generation, despite the source, almost all the produced energy is generated by electric generators. The wind power emulating test bench will use a synchronous motor and a generator. The theory in this chapter will focus on them and in more detail for permanent magnet synchronous machines (PMSM).

There has been a significant development past decades in the field of PMSM. The PMSM has various advantages compared to the IM and the PMSM has become a rival for IM in the field of industry, vehicles and household appliances. The reason for that is the PMSM does not need the magnetizing current in the rotor, because it is replaced by the permanent magnets (PM), which cause the needed excitation. The absence of excitation current causes higher power factor for PMSM than IM, minimizes rotor losses and removes the need of brushes [6]. Other advantageous sides compared to its counterparts are lower rotor inertia, which enables faster response, higher efficiency and compact structure. Also it has lower noise and vibration level. The disadvantages of the PMSM are its high cost of the permanent magnets, sensitivity to temperature rise and when PMSM operates in field weakening region, there is a possibility for saturation of the permanents magnets [5].

When using a permanent magnet synchronous generator (PMSG) in a wind turbine there are also multiple advantages compared to doubly-fed induction generator (DFIG). First of all PMSG is a direct-driven generator, which means there are no gears causing better efficiency and less maintenance. Wind turbines are connected to the distribution grid, which requires that the wind turbines must obey grid codes. The grid codes require that the wind turbines have low voltage ride through (LVRT) and fault ride through (FRT) capabilities. When having these capabilities, the wind turbine can stay connected to the distribution network during grid faults. During a grid fault they even have the capability to provide reactive power to the grid until it returns to normal. [7]

In Tampere University of Technology there was created another PMSG related wind turbine test system [8]. In that test system the wind was emulated by a DC-motor and the aim was to investigate the effect of voltage dips in wind turbines.

2.1 The working principle and the excitation of the SM

A radial-flux synchronous machine is a device, where the excited cylindrical rotor rotates inside the stator at the same time producing rotating magnetic field in the air gap between them. In a synchronous generator this rotating magnetic field induces a voltage to the stator windings [9]. The rotor is locked in the same frequency as the rotating magnetic field, hence the machine is called synchronous machine. As long as the supply frequency stays constant in synchronous motor, the rotor will rotate in constant frequency despite the load variations [10]. In Fig. 2.1 can be seen the main parts of interior PMSM (IPMSM).

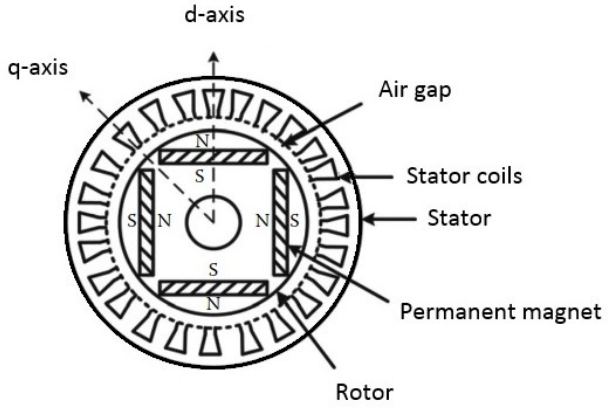

Figure 2.1. *Cross section of the interior type PMSM [11].*

When a synchronous motor is connected to the electric network, the speed of rotating magnetic flux in the air gap is the same as the frequency of the voltage in electric network, if there is no converter connected between them. The synchronous rotating speed can be calculated as

$$n_s = \frac{f}{p} \tag{2.1}$$

where f is the frequency of the voltage, which is applied to the stator and p is the number of pole pairs in the synchronous machine [9]. For example if the frequency is 50 Hz, the synchronous speed is then with a two pole machine 3000 rpm. SMs working areas can be divided into two sections based on their base speed. Beneath the nominal speed the machine operates in a constant torque region, where the magnetic flux remains constant. Above the nominal speed the machine operates in a field weakening region, where the magnetic flux decreases proportionately to speed. These control strategies will be discussed more at the Chapter 2.7.4.

It is important that there is constant magnetic flux in the rotor windings and it is implemented by the excitation. The excitation can be made in several ways in the rotor and it requires a DC current or permanent magnets. The most common way to do that is to carry the DC current from excitation equipment, which is attached to the rotor. The second way is to bring the DC current from outside of the synchronous machine via brushes. The third way is to bring the DC current from stator, but it causes other problems and consumes reactive power in the electric network. The fourth way is to replace the rotor windings by permanent magnets. Then the permanent magnets do not require DC current and the losses caused by the excitation are minimized. In the test setup permanent magnet machines will be used. [9]

2.2 Synchronous machine structure

The stator of SM consists of three-phase windings, which are surrounded by iron and shown in Fig. 2.2(b). The iron enables a good path for magnetic flux and it also has a good magnetic energy density in electromechanical interaction. This means that the magnetic fields can be processed like wanted. The good path for rotating magnetic fields in stator windings cause power losses by the eddy currents. To prevent that the iron is molded by laminated sheets, which reduces the losses. [9]

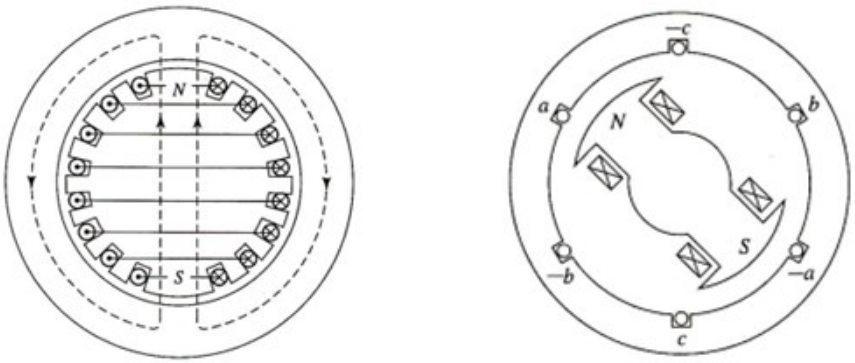

Figure 2.2. *The rotor types of synchronous machine, a) non-salient pole rotor b) salient pole rotor [9].*

As discussed earlier the rotor can be excited by the DC current or permanent magnets, but the rotor can be also divided into two groups based on how the rotor is constructed. In the Fig. 2.2(a) is a non-salient two-pole rotor, where windings are set in slots and divided in evenly along the whole ring. In the Fig. 2.2(b) is a salient two-pole rotor, where the windings can be easily seen from the pole shoes. The construction of the rotor is made the way that generated magnetic flux in the air gap is as sinusoidal as possible.

The windings of the rotor produce constant magnetic flux to the air gap, but the stator experiences an alternating sinusoidal flux, because the rotor is rotating. This causes an induction voltage to the stator and this phenomenon is based on the Faraday's law of induction. It is easier to create sinusoidal flux in the non-salient pole rotor, because the windings are divided in the slots and the distribution is even along the rotor ring. On the contrary, the sinusoidal flux is more difficult to achieve in the salient pole rotor, because the size of the air gap is not uniform in every spot. [9]

Synchronous machines with permanent magnets can be divided into axial and radial flux machines. In the axial flux machine the flux goes through magnets, which are parallel to the rotor shaft. This kind of machine is good for low rotating speeds, it is easy to make multipole and the diameter is large, hence it looks like a disc. In the radial flux machines the flux goes through magnets, which are perpendicular to the rotor shaft. This kind of machine is also good for low rotating speeds and it utilizes the best sides of the IM and SM, which mean having high torque on low speeds without gears. For example in paper mill application [12] there is a need for high torque in low rotating speed, which is suitable for radial flux PMSM. IM does not operate so well in low speeds without gearbox and low speed requires more poles, which would increase the size of the IM. Also efficiency and the power factor of the IM decrease, when the speed decreases. In the test bench will be used permanent magnet radial flux motor and generator. [9]

2.3 PMSM structure

PMSMs can be divided into two sections based on how the permanent magnets are installed in the rotor. The axes of rotor can be divided into direct and quadrature axes, which is a mathematical method to describe the permeances inside the rotor. These are called d- and q-axis. In the surface mounted permanent magnets the size of the inductances of the d- and q-axes are the same. The surface mounted permanent magnets are in Fig. 2.3(a), where can be seen that the magnets do not have any side supports. This can be a problem in high speed applications and applications where a high torque is needed. Therefore the permanent magnets are installed into slots and secured properly around the rotor. In Fig. 2.3(b) the interior magnets are inside the rotor, which are causing the inductances of the d- and q-axis separate a lot from each other. The characteristics of the PMSM can be influenced by locating the permanent magnets in different spots. [9]

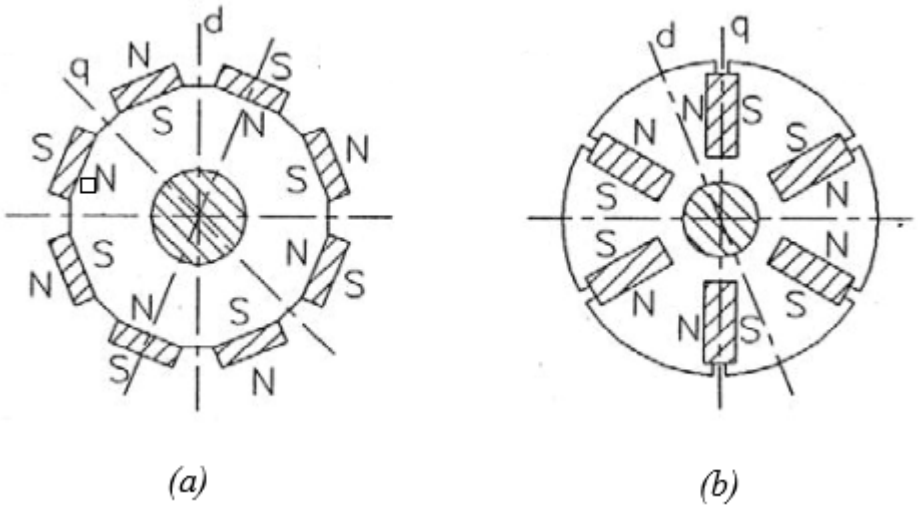

Figure 2.3. *The rotor types of PMSM, a) 8-pole surface-mounted magnets (b) 6-pole interior magnets [9].*

Materials used for permanent magnets have to be so called magnetic hard materials, because they are hard to demagnetize. It is important, because the demagnetization of PMs in PMSMs would cause severe problems to their operation. Ferrites were the first material used for PMs, because they were cheap, they had a high resistance and high operating temperature. But they had low remanence flux density and coercive field intensity. Better PM materials are aluminum-nickel-cobalt (AlNiCo), samarium-cobalt (SmCo) and neodymium-iron-boron (NdFeB). The last one is the most used material in PMSMs and its remanence flux density and coercive field intensity are higher than the others, but it does not bear as high temperature as the others. Coating magnets by nickel gives more temperature resistance, but also weakens the coercive field intensity of the magnets. It is also possible to mix PMs with plastic components, which makes them cheaper, but also weakens their magnetic characteristics. [9]

2.4 Space vector theory

The sinusoidal three-phase variables can be shown as one vector by using space vector theory, where the vector consists of real and imaginary parts [13]. The electric machines are constructed in a way that the rotating magnetic field between rotor and stator is as sinusoidal as possible. To use space vector theory, it is assumed that the voltages and currents in the electric machine are symmetrical and sinusoidal. Therefore, then the flux in the air gap can be assumed to be sinusoidal. The space vector theory is also a tool for analyzing and used for controlling the electric machines.

A three-phase system can be denoted by the following equation [13]:

$$\vec{v}_{abc} = \vec{v}_a + \vec{v}_b + \vec{v}_c = v_a e^0 + v_b e^{i\frac{2}{3}\pi} + v_c e^{i\frac{4}{3}\pi} \tag{2.2}$$

where $e^{i\frac{2}{3}\pi} = \alpha = 1\angle 120°$ and it is known as Fortescue operator. v_a, v_b and v_c are phase voltages of a three-phase system. Using Fortescue operator the equation gets a new form:

$$\vec{v}_s = \frac{2}{3}(v_a + \alpha v_b + \alpha^2 v_c) = v_s e^{i\theta} \tag{2.3}$$

where coefficient $\frac{2}{3}$ is for keeping the length of space vector same as the peak value of voltage or current, but the coefficient can vary based on the application, for example in constant power transformation the coefficient is $\sqrt{\frac{2}{3}}$. v_s is the magnitude and θ is the angle of space vector.

A three-phase coordinate system can be changed to a two-axis coordinate system by Clarke's transformation. The two-axis coordinate system is a more convenient way to represent variables. Complex variables can be divided into real (α) and imaginary (β) components. The $\alpha\beta$-coordinate system is also known as a stationary reference frame. The Clarke's transformation is based on Euler's formula [13]:

$$e^{i\theta} = \cos(\theta) + i\sin(\theta) \tag{2.4}$$

$$\begin{bmatrix} v_\alpha \\ v_\beta \end{bmatrix} = \frac{2}{3}\begin{bmatrix} 1 & -\frac{1}{2} & -\frac{1}{2} \\ 0 & \frac{\sqrt{3}}{2} & -\frac{\sqrt{3}}{2} \end{bmatrix}\begin{bmatrix} v_a \\ v_b \\ v_c \end{bmatrix} \tag{2.5}$$

where v_α is the real part and v_β is the imaginary part of the space vector. The best way to analyze electric machines is to use synchronous reference frame, in which the controlled variables are DC variables. Therefore conventional PI-controllers are possible to use in the control system. Depending on the electric machine the frame might vary, but in synchronous machines the frame is set to the rotor reference frame.

The transformation from three-phase variables to synchronous reference frame is known as Park's transformation. The transformation from stationary reference frame to synchronous reference frame is in matrix form:

$$\begin{bmatrix} v_d \\ v_q \end{bmatrix} = \begin{bmatrix} \cos(\delta) & \sin(\delta) \\ -\sin(\delta) & \cos(\delta) \end{bmatrix}\begin{bmatrix} v_\alpha \\ v_\beta \end{bmatrix} \tag{2.6}$$

where v_d and v_q are the space vectors in dq-coordinate system. δ is the angle between v_α and v_d. The Park's transformation matrix [13] is formed by the following

$$\begin{bmatrix} v_d \\ v_q \end{bmatrix} = \frac{2}{3}\begin{bmatrix} \cos(\delta) & \cos(\delta - \frac{2}{3}\pi) & \cos(\delta + \frac{2}{3}\pi) \\ \sin(\delta) & \sin(\delta - \frac{2}{3}\pi) & \sin(\delta + \frac{2}{3}\pi) \end{bmatrix}\begin{bmatrix} v_a \\ v_b \\ v_c \end{bmatrix} \tag{2.7}$$

From Fig. 2.4 can be seen the three-phase voltages, stationary reference frame variables and synchronous reference frame variables. v_s in the Fig. 2.4 is the voltage vector in dq-coordinate system.

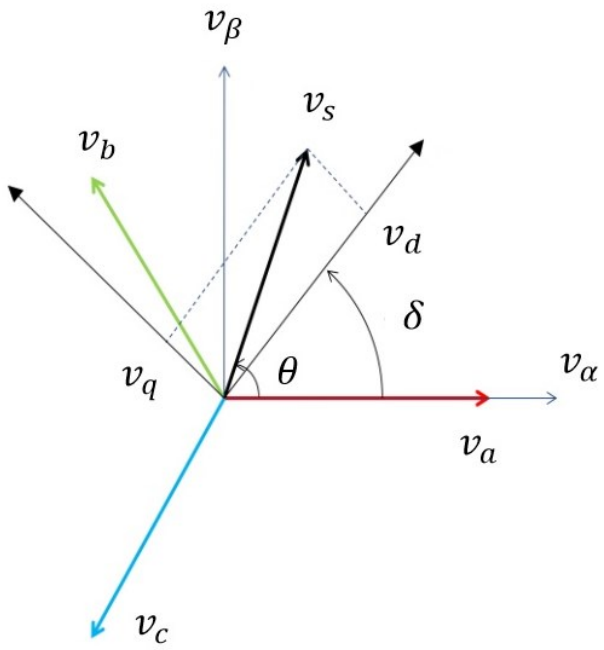

Figure 2.4. *The complex plane shows abc-, $\alpha\beta$- and dq -coordinate systems [modified 13].*

It should be noted that $\alpha\beta$- and dq-coordinate systems do not represent any actual physical variables. They are only a clever way to model and control the electric machines. [13]

2.5 Dynamic model of salient pole PMSM

The equivalent circuit of a PMSM is more complicated than non-salient synchronous machine. The saliency is caused by the asymmetrical inductances in direct axis L_{sd} and quadrature axis L_{sq} in the following equations. The subscript "s" refers to stator, but the equations are seen in rotor reference frame [14]. Throughout of this thesis, the following

assumptions are made: the induced EMF is sinusoidal, eddy currents and hysteresis effect are neglected, three-phase supply voltages are balanced and air-gap reluctance has sinusoidal and constant components [15].

$$L_{sd} = L_{md} + L_{ls} \tag{2.8}$$

$$L_{sq} = L_{mq} + L_{ls} \tag{2.9}$$

where L_{md} is the magnetizing inductance of the d-axis and L_{mq} is the magnetizing inductance of the q-axis. L_{ls} is the leakage inductance caused by the stator windings. The stator experiences a different inductance depending on the rotor position. Using inductances above, the flux linkage of the d-axis Ψ_{sd} and q-axis Ψ_{sq} are determined:

$$\Psi_{sd} = L_{sd} i_{sd} + \Psi_{pm} \tag{2.10}$$

$$\Psi_{sq} = L_{sq} i_{sq} \tag{2.11}$$

where i_{sd} and i_{sq} are the stator currents of dq-axes. Using inductances and flux linkages shown above can be determined the d-axis v_{sd} and q-axes v_{sq} stator voltages by the following:

$$v_{sd} = R_s i_{sd} + \frac{d}{dt}\Psi_{sd} - \omega_e \Psi_{sq} \tag{2.12}$$

$$v_{sq} = R_s i_{sq} + \frac{d}{dt}\Psi_{sq} + \omega_e \Psi_{sd} \tag{2.13}$$

where R_s is the resistance of the stator winding and ω_e is rotor angular electrical speed [14]. The terms $\frac{d}{dt}\Psi_{sd}$ and $\frac{d}{dt}\Psi_{sq}$ are caused, because the flux linkage varies as a function of time. The terms $\omega_e \Psi_{sd}$ and $\omega_e \Psi_{sq}$ are caused, because the coordinate system rotates as for the stator windings [16]. In Fig. 2.5 the equivalent circuits differ from each other due the fact that permanent magnet excitation is aligned to d-axis.

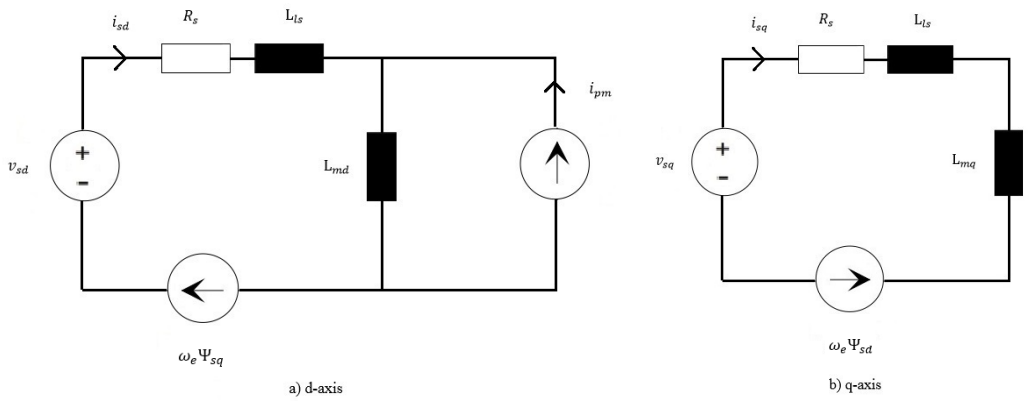

Figure 2.5. *The equivalent circuits of a salient pole PMSM a) d-axis b) q-axis [modified 17].*

The produced instantaneous electrical torque T_e [16] is divided to a torque term, which is based on the PM excitation, and the other term which is known as reluctance torque. The reluctance torque equals to zero, if the inductances of dq-axes of the machine are the same.

$$T_e = \frac{3}{2} p\left[\Psi_{pm} i_{sq} + i_{sq} i_{sd} (L_{sd} - L_{sq})\right] \tag{2.14}$$

An equation of motion determines whether the rotor turbine accelerates, decelerates or operates with constant speed. The equation of motion is defined as:

$$T_e - T_L = J \frac{d\omega_{mec}}{dt} + B\omega_{mec} \tag{2.15}$$

where T_e is the electromagnetic torque, T_L is the mechanical torque reduced to the generator shaft, J is the total inertia of the wind turbine system reduced to the generator shaft. ω_{mec} is the mechanical angular velocity of the rotor and B takes into account the losses proportional to the rotational speed, which is known as friction coefficient. As can be seen from (2.15) the produced electrical torque has to overcome the load torque and the losses caused by rotation and inertia of the rotor.

2.6 Wind turbine model

The wind turbines convert mechanical energy to the electrical energy, when air flow goes through the cross-sectional area of blades at the same time rotating the generator in the wind turbine. The amount of energy, which is converted depends on the characteristics of the wind turbine and the wind speed. At the beginning of the twentieth century Albert Betz showed [18] that the power produced by the wind turbine is based on the wind speed

and the cross-sectional area of the blades [16]. The following equations are derived from kinetic energy and mass flow of the air, which go through the cross-sectional area of blades. He showed that the produced power depends on the ratio between the wind speed in front of the blades and after the blades, but in this thesis that will not be modelled.

$$P = \frac{1}{2} c_p(\lambda_w, \theta_w) \rho A v_w^3 \tag{2.16}$$

$$\lambda_w = \frac{r \omega_{mec}}{v_w} \tag{2.17}$$

where ρ is the air density, A is the cross-sectional area the blades and v_w is the wind speed. c_p is the utility coefficient, influenced by the wind turbine characteristics and the wind speed. λ_w is known as the tip speed ratio and θ_w is the blade angle. r in the equation is the length of the blade. Small tip speed ratio does not give as much power as possible, but on the other hand too big tip speed ratio generates losses and reduces the total power of the wind turbine [16].

The power equation is rough estimation for produced power, because it is assumed that the air flow is frictionless, but it is accurate enough for engineering purposes. In the test bench real wind will not be used, but it is emulated by the motor, which will be modelled as it would have an input by the wind speed.

Fig. 2.6 illustrates the maximum power of the wind turbine as a function of the wind speed. A practical wind turbine has a threshold for wind speed, when it starts to rotate and an end wind speed, where it is turned off in a controlled way. These points are marked as cut-in and cut-off wind speeds. The cut-off wind speed is required for protecting mechanical and electric parts of the wind turbine. The control is done so that the power received would be maximum and it is achieved under the nominal wind speed by using optimal tip speed ratio and maximum utility coefficient. This is known as maximum power point tracking (MPPT) algorithms. Over nominal wind speed the maximum power has to be restricted and it is done by using pitch control. [16]

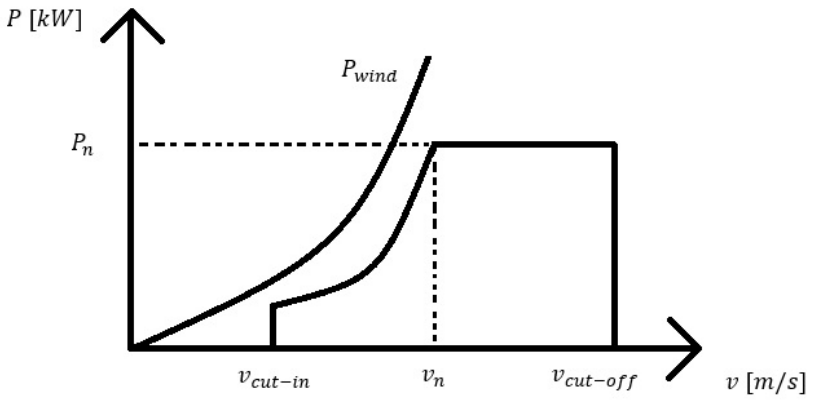

Figure 2.6. *The control principle of the wind turbine, which is based on the wind speed [modified 16].*

The pitch control is a mechanism to reduce power of wind turbine by changing the blade angles. It is done by either electro-mechanical or hydraulic actuators. It is only used, when wind speeds go over nominal in large scale wind turbines, usually smaller ones do not have it. The pitch control is part of control system family, which consists of controlling of rotor speed, yaw, power and operational sequence. These are not discussed any further, because the real test bench does not include any of these control mechanisms [18].

2.7 The control of PMSM

In this chapter is discussed about the control system of PMSM. It requires three-phase two-level frequency converters, a vector control system, a modulation technique required for power switches and optimal control strategies.

2.7.1 The AC-DC-AC converter

The basic scheme of AC-DC-AC converter needed for wind turbine test bench is in Fig. 2.7. It is known as three-phase two-level frequency converter with an LCL filter. It consists of an AC-DC converter and a DC-AC inverter with a DC-link capacitor between them. Insulated gate bipolar transistors (IGBT) are used as switches and they are controlled by sinusoidal pulse width modulation (SPWM), which is discussed in chapter 2.7.3. The converter offers bidirectional power flow, when there are anti-parallel diodes attached with the IGBTs.

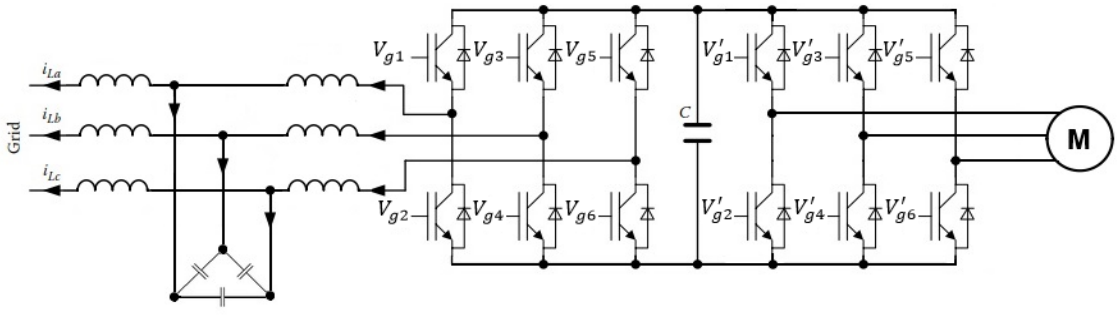

Figure 2.7. *Three-phase two-level frequency converter.*

Fig. 2.7 shows only the motor side converter and LCL filter, even though the generator side is exactly the same. The LCL filter consists of two inductors and one capacitor for each phase, where the capacitors are connected to delta. The filters are needed for reducing the voltage and current ripples to the grid. There are several filter options available, but in this test bench will be used an LCL filter instead of an LC filter or an L filter.

2.7.2 Vector control

There are multiple control methods available for different applications and machine types. A basic control method is a scalar control, which is also known as V/f-control. In the scalar control the ratio between supplied voltage and frequency are kept constant and it is useful in applications, where are not needed high dynamics in control, for example pumps and fans. A more sophisticated control method is Direct Torque Control (DTC). By that control method is possible to control stator flux linkage and electromagnetic torque separately. DTC has also good torque dynamics and the switching frequency is variable [19].

By vector control is also possible to control stator flux linkage and torque separately like was in DTC. It is also called as Field Oriented Control (FOC). Vector control is based on controlling currents in dq-rotating reference frame and the control scheme is in Fig. 2.8. The variables marked as star '*' in Fig. 2.8 refer to reference value and without the star the variables are measured values.

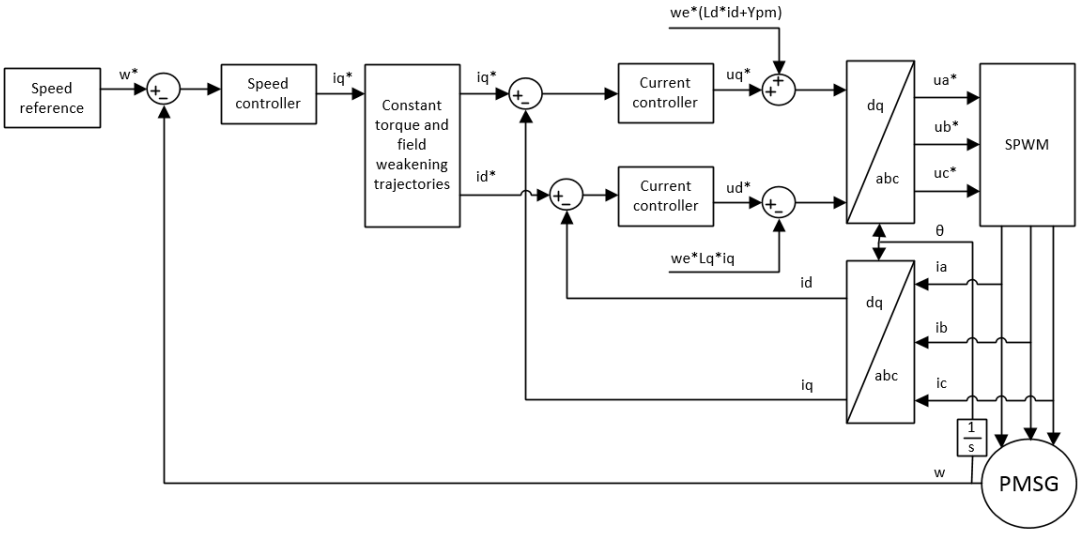

Figure 2.8. *The vector control scheme of the PMSG.*

In Fig. 2.8 there is a simplified model of the vector control system. The output of the PMSG is the measured angular velocity, which is subtracted from the speed reference. This error variable is the input for the PI-speed controller, which gives the i_q-current reference. The i_d-current reference is determined by the control strategies, which are presented in Chapter 2.7.4. After the right control strategy is selected, the PI-current controllers will receive i_d- and i_q-current references, from which are subtracted the measured i_d- and i_q-currents. The outputs of the current controllers are u_d- and u_q-voltage references. To achieve decoupled control of the dq-axes, there is a need for decoupling signals to be added or subtracted from u_d- and u_q-voltage references. These voltages are transformed to three-phase variables by the inverse Park's transformation, which was introduced in Chapter 2.4. After the transformation, the voltages will be sent to sinusoidal pulse width modulation, whose outputs are the control pulses for IGBTs. The measured three-phase currents are transformed to dq-variables by the Park's transformation. The transformation blocks require knowledge of the rotor position in every moment. It is received from the integral of the measured angular velocity. A more detailed model will be presented in Appendix A.

2.7.3 Sinusoidal pulse width modulation

The aim of the two-level frequency converter is to convert AC-voltage to DC-voltage and DC-voltage to AC-voltage. Succeeding in that, the power switches in the inverter need to be controlled. It can be made by a switching technique, which is called as pulse width modulation technique (PWM). The main idea of PWM is to chop the DC-voltage to pulses, which have different pulse widths. By controlling these pulse widths it is possible to control the output AC-voltage to have the desired amplitude and frequency. There are multiple PWM techniques available, but one of the most common used in industry is the

sinusoidal pulse width modulation. In SPWM technique there is a modulating signal, which is sinusoidal and a carrier signal, which is triangular. When this modulating signal is larger than the carrier signal, the result is a pulse, which is known as on-time. If it is smaller, it does not give any pulse and it is known as off-time. Each generated pulses trigger their respective power switch, which name can be seen from Fig 2.7 and Fig. 2.9. Vg1, Vg3 and Vg5 are the upper switches of the inverter and when they conduct, then the inverter output is $\frac{V_{dc}}{2}$ as can see from equation (2.20). On the contrary Vg2, Vg4 and Vg6 are the lower switches of the inverter and when they conduct, the inverter output is $-\frac{V_{dc}}{2}$. Fig. 2.9 is made for three-phase modulating signals, which have 120 degrees phase shift and a frequency of 50 Hz. The carrier frequency is 1 kHz and the modulation index is 0.8. Under the SPWM signal are seen the pulses, which are generated by the SPWM and then forwarded to the upper and the lower switches. [20]

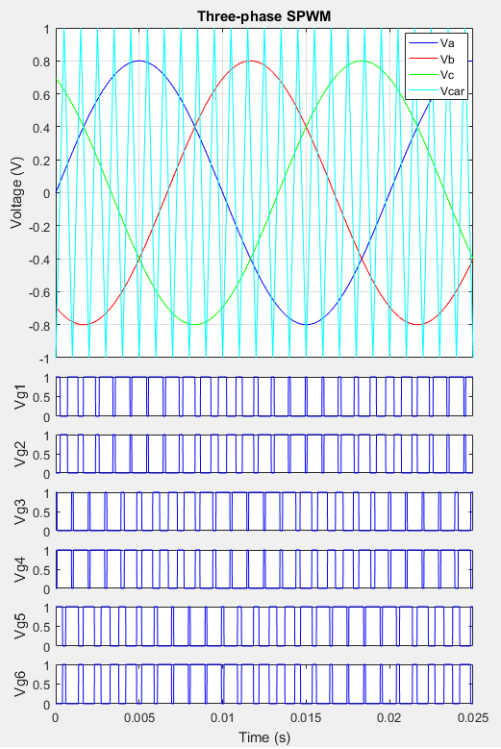

Figure 2.9. *Sinusoidal pulse width modulation.*

The frequency of the carrier signal is usually a multiple of the modulating signal. The LCL filter and motor inductance filters out the current harmonics, which occur at the switching frequency and its multiple. The higher the switching frequency is, the more switching losses are generated. [21]

The ratio between modulating and carrier signal's amplitudes are known as modulation index. Modulation index expresses the capability of the inverter to utilize the DC-

voltage [22]. When modulation index is between 0 and 1, then it is said that modulation works in linear operation, if it goes above that, then the modulation goes to non-linear operation [22]. The modulation index is usually under 1, because then the SPWM works properly. If the modulation index goes above 1, then it is called as overmodulation. Sometimes overmodulation is allowed to reach higher AC-voltages, but it also weakens the quality of the output voltages [21]. Modulation index is

$$m_a = \frac{A_m}{A_c} \tag{2.18}$$

where A_m is the amplitude of the modulating signal and A_c is the amplitude of the carrier signal. Modulation index can be also determined by using frequencies:

$$m_f = \frac{f_m}{f_c} \tag{2.19}$$

where f_m is the frequency of the modulating signal and f_c is the frequency of the carrier signal. The inverter's output phase voltage (RMS) value is determined by the following:

$$V_{a(RMS)} = \frac{V_{dc}}{2} \tag{2.20}$$

The maximum of the linear modulation region and line-to-line output voltage (RMS) of the inverter can be determined by using phase voltage as:

$$V_{ab(RMS)} = \sqrt{\frac{3}{2}} V_{a(RMS)} = \frac{1}{2}\sqrt{\frac{3}{2}} V_{dc} = 0.612 V_{dc} \tag{2.21}$$

The theoretical maximum in nonlinear modulation region and line-to-line output voltage of the inverter is then:

$$V_{maxab(RMS)} = \frac{V_{a(RMS)}}{V_{fund}} = \frac{\frac{V_{dc}}{2}}{\frac{2V_{dc}}{\pi}} = \frac{\pi}{4} = 0.785 V_{dc} \tag{2.22}$$

where V_{fund} is the fundamental wave of the square wave signal. There are solutions to improve the DC-voltage utilization. For example third harmonic injection [22], which increases the linear operation range to $m = 1.15$.

2.7.4 Control strategies

The high efficiency working interior permanent magnet synchronous machine requires a control strategy, where it has a wide range of speed and the stator current losses are minimized. It is achieved by a high performance working drive with maximum torque per ampere (MTPA) control technique for low speeds and an ability for field weakening in high speeds [23]. Thus, the control strategies can be divided into sections based on the machine's nominal speed. In Fig. 2.10(a) are constant torque and constant power regions. In the constant torque region the machine will receive maximum torque from zero to nominal speed. In the same time power and supply voltage is increased linearly. On the other hand after the machine's speed goes over nominal speed, the machine will go to constant power region, which is also known as field weakening region. In that region the torque is decreased proportional to the speed while power and supply voltage are kept constant.

2.7.4.1 Constant torque region

By using MTPA control technique in the constant torque region the stator currents are minimized. Therefore the power losses in the IPMSM windings are also minimized. The maximum torque can be calculated by using the electrical torque equation (2.14) and finding the optimal value for stator current angle. In polar form stator current is

$$I_s \angle \gamma = I_s \cos(\gamma) + jI_s \sin(\gamma) = i_{sd} + ji_{sq} \tag{2.23}$$

where γ is the stator current angle. Equation (2.24) is formed by substituting current component values in (2.14) by stator current magnitude with current angle from (2.23). Then this second degree equation is partial differentiated as for the current angle and setting the result to zero [24]:

$$\frac{\partial T}{\partial \alpha} = \frac{3p}{2} \Psi_{pm} I_s \sin(\gamma) + \frac{3p}{2} \left(L_{sd} - L_{sq}\right) I_s^2 \frac{\sin(2\gamma)}{2} = 0 \tag{2.24}$$

As mentioned earlier the terms of the torque equation can be divided into magnetizing term and reluctance term. Those are in Fig. 2.10(b), where the both torque terms are drawn, when using the nominal values of stator current with different current angles. In theory the magnetizing term the optimum current angle is 90° and for reluctance term that maximum current angle is 135°, which means that the optimum current angle somewhere between them.

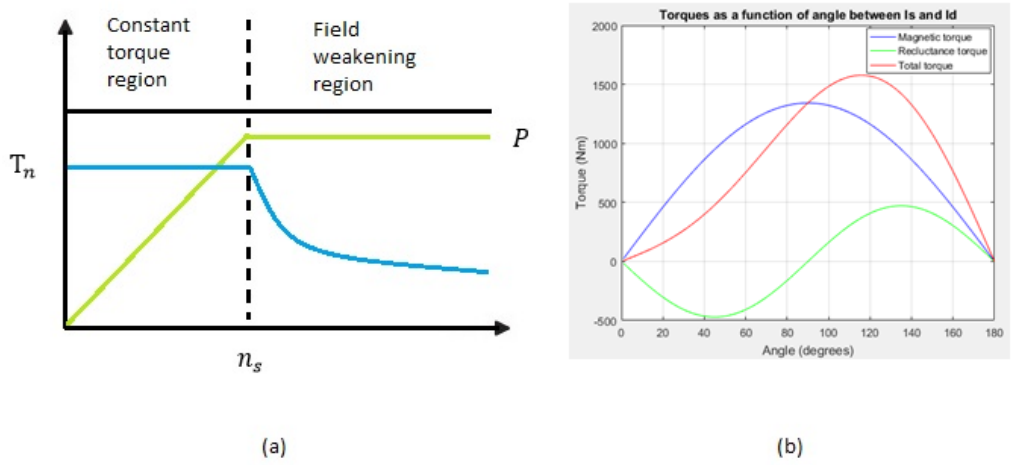

Figure 2.10. *(a) The constant torque and field weakening regions as a function of speed (b) the maximum torque as a function of the current angle.*

The control algorithm of the MTPA determines first the arbitrary value of stator current component i_{sq}, which is inside the limits and received from speed controller [25]. After i_{sq} is determined, it can be used for calculating the value of stator current component i_{sd}. After (2.24) is partial differentiated, then it is possible to remove the angles and use only dq-currents. After the derivation [26] the following is achieved:

$$i_{sd} = \frac{\Psi_{pm}}{2(L_{sq} - L_{sd})} - \sqrt{\frac{\Psi_{pm}^2}{4(L_{sq} - L_{sd})^2} + i_{sq}^2} \tag{2.25}$$

The current component values cannot be arbitrary. There are maximum values for both currents and voltages of the IPMSM. The constraints are introduced by the following:

$$I_s = \sqrt{i_{sd}^2 + i_{sq}^2} \leq I_{sm} \tag{2.26}$$

$$V_s = \sqrt{v_{sd}^2 + v_{sq}^2} \leq V_{sm} \tag{2.27}$$

where I_{sm} is the maximum stator current of IPMSM. V_{sm} is the maximum voltage of the IPMSM, which is restricted by DC-link voltage. From Fig 2.11 can be seen the voltage and current constraints determined in equations (2.26)-(2.27) and drawn in the dq-complex plane. The voltage limit loop is an ellipse and it is different for every angular speed even if only one ellipse is drawn. On the other hand, the circular current limit loop is static, because the maximum allowed stator current remains constant. In Fig. 2.11 can

also be seen a theoretical MTPA -curve, which is also known as optimum MTPA trajectory. The real trajectory used in control is named in the figure as actual MTPA curve, because it is inside the current limits. This optimum MTPA trajectory should be obeyed, when controlling IPMSM in low speeds.

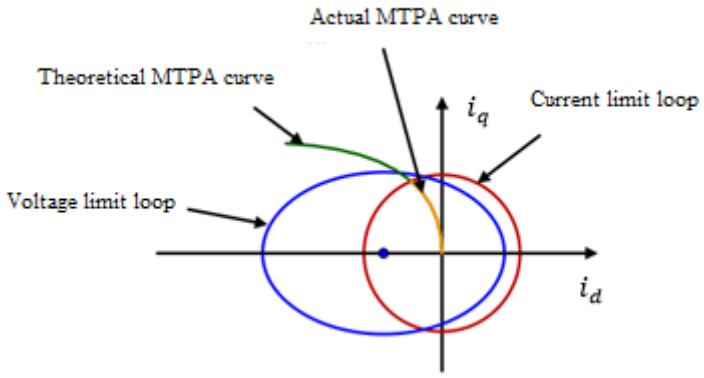

Figure 2.11. *Optimal MTPA trajectory with constraints [modified 23].*

The maximum values for the current limit loop are determined as [25]:

$$I_{smd} = \frac{\Psi_{pm}}{4(L_{sd} - L_{sq})} + \sqrt{\frac{\Psi_{pm}^2}{16(L_{sd} - L_{sq})^2} + \frac{I_{sm}^2}{2}} \tag{2.28}$$

$$I_{smq} = \sqrt{I_{sm}^2 - I_{smd}^2} \tag{2.29}$$

where I_{smd} is the maximum allowed d-axis current component and I_{smq} is the maximum allowed q-axis current component. These limits have to be implemented into Simulink model, where the optimal trajectories are calculated.

2.7.4.2 Field weakening region

Controlling PMSM in the field weakening region is more complex than it is in constant torque region. In constant torque region the current limits were the dominant and restricted the optimum MTPA trajectory. In the field weakening region it is the opposite, because according to (2.30), when angular velocity becomes higher, the voltage limits are getting smaller. That is the reason why MTPA technique cannot be used anymore in the

field weakening region. Fig 2.12 verifies that, where the flux weakening curve goes along with the voltage limit ellipse.

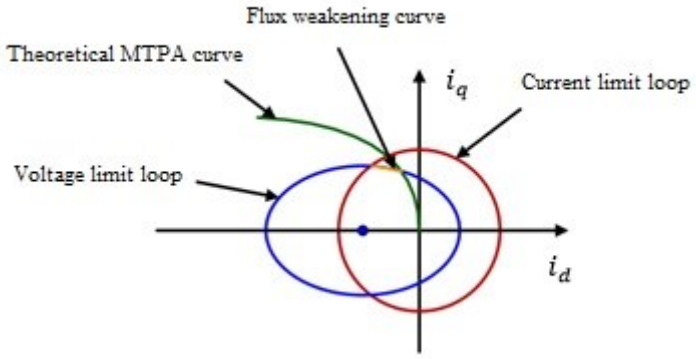

Figure 2.12. *Field weakening control with constraints [modified 23].*

In field weakening control the basic idea remains the same as was in the MTPA technique, except that the stator voltage is kept constant and in its maximum value. According to the flux weakening control technique the current component i_{sq} is first determined as an output of speed controller as in MTPA technique. At the same time the total air gap flux is weakened by i_{sd} [24]. Thus, it is possible to increase the angular velocity at the same time, when stator voltage is kept constant. After that the d-axis current component i_{sd} can be solved by the following [25]:

$$\sqrt{(L_{sd}i_{sd} + \Psi_{PM})^2 + (L_{sq}i_{sq})^2} \leq \frac{V_{sm}}{\omega_e} \tag{2.30}$$

By solving i_{sd} from the previous equation, it will form a second degree equation. After the derivation the equation look like [25]:

$$i_{sd} = -\frac{\Psi_{pm}}{L_{sd}} + \frac{1}{L_{sd}}\sqrt{\frac{V_{om}^2}{\omega_e^2} - (L_{sq}i_{sq})^2} \tag{2.31}$$

where $V_{om} = V_{sm} - R_s I_{sm}$ when the stator resistance is neglected. When i_{sd} decrease the flux in the air cap, there are a possibility for current saturation in high speeds. It is prevented by using current limits [25], where I_{smd} is the d-axis current constraint and determined by the following:

$$I_{smd} = -\frac{\Psi_{pm}L_{sd}}{a} + \frac{1}{a}\sqrt{\Psi_{pm}^2 L_{sd}^2 - ab} \tag{2.32}$$

where $a = L_{sd}^2 - L_{sq}^2$ and $b = I_{sm}^2 L_{sq}^2 + \Psi_{pm}^2 - \frac{V_{sm}^2}{\omega_e^2}$. The current constraint I_{smq} can be calculated in the same way as in (2.29). The equations and the Simulink model for completing flux weakening control technique can be found from Appendix A.

3 CONSTRUCTION OF THE SYSTEM

This chapter contains a report of what kind of wind turbine test bench was built and what was the idea behind it. It includes the reviewing of machines, converters, filters and how they are installed. The chapter ends of showing the complete system.

3.1 The structure of the system

The implemented system consisted of a motor and a generator, which had a torque transducer between them as can see from Fig. 3.1. The motor and the generator are controlled by two-level power converters. In a commercial power converter diode rectifiers are used. Therefore, the other power converter is used to operate as a grid converter enabling bidirectional power flow. The DC circuits of both converters are connected together and the diode rectifiers are bypassed. However the diode rectifiers are used for charging the DC capacitors during start up. Two LCL filters were required to enhance the power quality and they were installed in both ends.

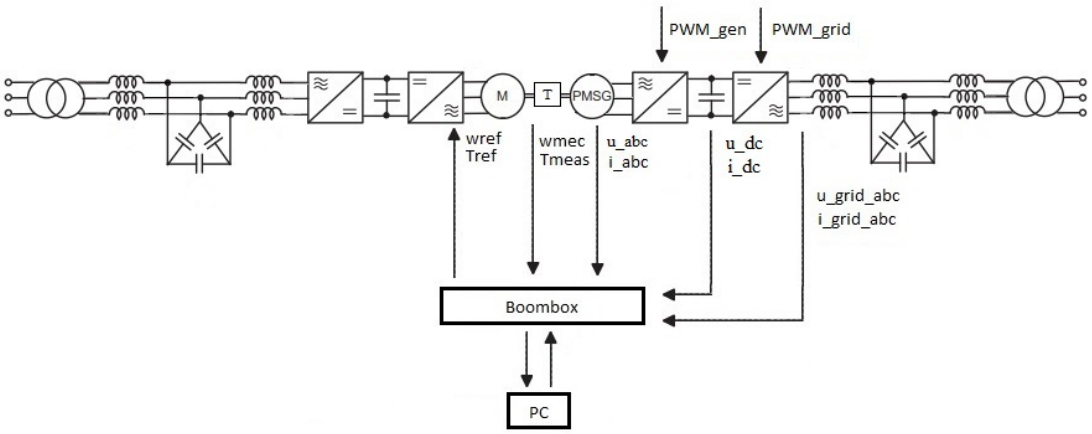

Figure 3.1. *Graphical illustration of the whole system with measurements.*

To emulate wind turbine operation, the idea is to give a wind speed input to the motor, which converts that input to torque. The input torque defines the input speed for generator, which is developed by MPPT-algorithm and is not done in this thesis. In the motor side a control system by Danfoss is used and in the generator side our own controls.

All the inputs and outputs of the system come from a hardware and a software named Boombox, which is a rapid control prototyping platform. It allows to transform Simulink models to C-language, but due the schedule reasons there were no time to im-

plement the software part of Boombox in this thesis. That is why only the ordered measurement circuits are installed. The installed measurements are generator's currents and voltages, DC current and voltage, grid side currents and voltages.

3.2 Motor and generator

The motor and generator used for the test bench are radial flux salient pole PMSMs with six pairs of poles. They look exactly same except that the generator has measurement windings, which required an extra box aside the generator. The measurement windings are used for more precise investigation of the windings inside the stator. The data received from measurement windings are used for modeling the windings numerically. The material used for machines are cast iron and welded steel. The mass of one machine is 680 kg and both have equal mass. Their electrical characteristics are in Table 3.1 and the machines are in Fig. 3.2.

Table 3.1. *Electrical characteristics of motor and generator.*

	Motor	Generator
P_n	17 kW	13.5 kW
V_n	370 V	370 V
f_n	12.7 Hz	12.7 Hz
n_n	127 rpm	127 rpm
I_n	34 A	33.1 A
$\cos(\varphi)$	0.96	0.65
T_n	1279 Nm	1016 Nm
p	6	6

The nominal speed is 127 rpm as shown in Table 3.1, which is kind of slow speed while the nominal torque is up to 1279 Nm. The reason for low speed was to eliminate the need of gears. Thus, they work as direct driven machines, when the frequency converters are directly coupled to the machines.

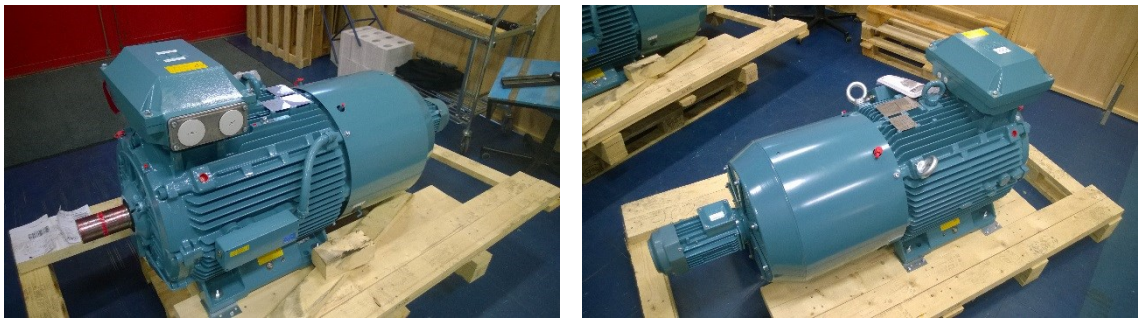

(a) *(b)*

(c)

Figure 3.2. *The used machines: (a) generator, (b) motor and (c) when both are installed in the test bench.*

The machines are connected together via mechanical couplings as seen from Fig. 3.2(c). When installing the machines in the bench, it was critical that the machines were aligned with each other. The mechanical couplings, which we used allowed a very small error in misalignment. The mechanical couplings are known also as flexible claw clutches.

The machines can be used in either star connection or in delta connection. The machines are used in star connection in the test bench, and their equivalent characteristics can be seen from Table 3.2.

Table 3.2. *Equivalent circuit characteristics in star connection.*

	Motor	Generator
R_s	700 mΩ	700 mΩ
L_d	56 mH	56 mH
L_q	71 mH	71 mH
Ψ_{pm}	3.18 Wb	3.18 Wb

In Table 3.2 can be seen stator resistance, direct- and quadrature-axis inductances and the flux linkage produced by the permanent magnets. These information are found from machine plate except for the flux linkage, which was calculated mathematically.

3.3 Converters

The converters used in the test bench were ordered from Danfoss Drives. The ordered converters are two-level frequency converters, overall four converters and two of them have different I/O-boards than the other two. The type codes are NXP00615A2H1SSSA8A2A5D3D2 and NXP00615A2H1SSSA8A200D300. The meaning of those type designations can be found from Table 3.3. The zero parts (00) in the type code are equivalent to empty board.

Table 3.3. *Explanations of the type designations.*

Description	Meaning
NXP	Model - excellent performance
0061	Nominal current 61 A
5	Nominal voltage 380-500 VAC
A	Basic graphical panel
2	IP21
H	IEC/EN 61800-3
1	Internal brake chopper without resistance
S	6-pulse connection
S	Air-cooled
S	Basic boards
A8	Vacon NX basic I/O board
A2	Standard Vacon NX relay board
A5	Vacon NXP encoder board
D3	RS-232 adapter board
D2	Vacon NXP system bus adapter board

According to Table 3.3, the nominal current of the converter is 61 A. Additional DC brake chopper is required, if the motor is wanted to decelerate and if the diode rectifier of the converter is used instead of active rectifier. Option board A2 and additional contactor are used to control the charging of the DC-link capacitors through diode rectifier before the start-up of the active rectifier. The torque reference and speed limit are created in the self-made control system and these will be given to the converter from the Boombox through option board A8. The Active Front End (AFE) control system of Danfoss is implemented to the grid side converter. It requires option board D7, which includes Phase-Locked Loop (PLL) to synchronize output voltage to grid voltage and measured

by an additional measurement transformer. From Fig. 3.3 can be seen a picture of all the converters, when they are installed in the wall.

Figure 3.3. *Vacon NXP converters. The first two from left side are generator side converters, the two in the right side are motor side converters.*

The VaconBus adapter boards are added in the generator side converters as shown in Fig. 3.3. They separate the power part and control part from the converter. Therefore, the main reason for the adapter boards for us is that, they are required to bypass Danfoss control system and replace it by our own control system. The VaconBus adapter boards have seven fiber-optic PWM inputs, whose descriptions can be seen from Table 3.4.

Table 3.4. *Explanations of the fiber-optic PWM inputs of the VaconBus adapter [27].*

Fiber number	Signal	Description
1	Enable	Activates operation of the switches
2	U-phase	Controls U-phase switches
3	V-phase	Controls V-phase switches
4	W-phase	Controls W-phase switches
5	AD-converter	Starts AD-conversions in VaconBus power part
6	VaconBus RX	Serial data receive
7	VaconBus TX	Serial data transmit

In Table 3.4 the first fiber is used for enable signal. Boombox does not require that, because it can disable and enable automatically the PWM outputs, when needed. Fiber numbers 2-4 are required to control switches and they are connected between Boombox outputs and VaconBus adapter. Boombox transmits only the commands to the higher switches, VaconBus adapter can invert them to the lower switches. Fiber numbers 5-7 are required for AD-conversion and data transmitting between control part and power

part. Hence they are connected between VaconBus adapter and the fiber board behind the control panel.

3.4 LCL filters and the sizing of the damping resistors

The LCL filter consists of two different size inductors and capacitors, which are connected to the three-phase network. The capacitors are connected to delta. They are placed between the converter and grid and named according to that. LCL filters are needed for attenuating the switching harmonics caused by voltage source converters (VSC) [28]. In the circuit inductor is needed for attenuating low order harmonics and reducing current ripples [29]. LCL filter also boosts the currents, which ensures the proper operation of grid converter. The size of inductors is relatively big, because they have high current capability, but low inductance values, which are shown in Table 3.5. The capacitor in the LCL filter provides a low resistance path for high order harmonics [29]. Hence the capacitor is good for attenuating harmonics at high frequencies. The filters were ordered from Danfoss, but they came from a German company named Platthaus GmbH and they can be seen as installed from Fig. 3.4.

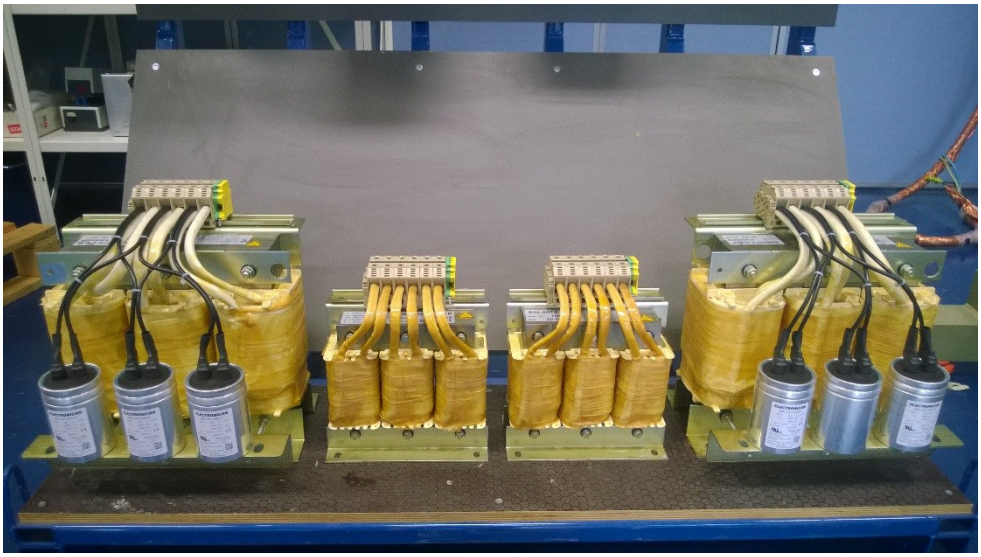

Figure 3.4. *LCL filter in right is generator side and the left LCL filter is the motor side.*

Table 3.5. *The characteristics of LCL-filter inductors and capacitors.*

Grid side inductor	L_g	0.54 mH
Converter side inductor	L_c	1.08 mH
Delta connected capacitors	C_f	16 μF

To produce a single-phase equivalent circuit for the LCL filter, delta-star transformations are needed, which are presented in Fig. 3.5. Usually these passive elements

are showed by using impedances, but in here capacitances are used. The transformation from impedance to capacitance is $Z = 1/(j\omega C)$, but in the following equations imaginary part j and angular frequency ω can be eliminated.

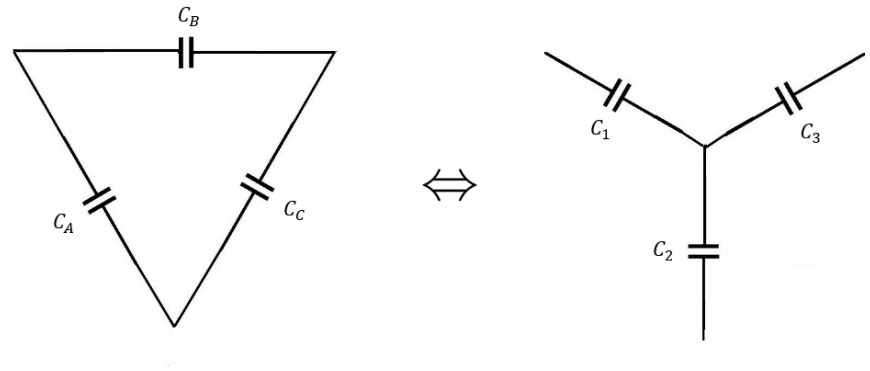

Figure 3.5. *Delta-star transformation for capacitors.*

Using impedances and capacitances the transformation from delta connection to star connection are determined by the following:

$$Z_1 = \frac{Z_A Z_B}{Z_A + Z_B + Z_C} \Leftrightarrow Z_Y = \frac{Z_\Delta^2}{3Z_\Delta} \Leftrightarrow Z_\Delta = 3Z_Y \tag{3.1}$$

$$\frac{1}{C_1} = \frac{\frac{1}{C_A}\frac{1}{C_B}}{\frac{1}{C_A} + \frac{1}{C_B} + \frac{1}{C_C}} = \frac{C_C}{C_B C_C + C_A C_C + C_A C_B} \Leftrightarrow$$
$$\frac{1}{C_Y} = \frac{C_\Delta}{3C_\Delta^2} \Leftrightarrow C_Y = 3C_\Delta \tag{3.2}$$

Equations show symmetrical impedance and capacitance transformations. As the result for symmetrical passive elements, the delta connected impedances are triple compared to star connected impedances. On the contrary star connected capacitances are triple compared to delta connected capacitances.

The LCL filter produces resonance between inductive and capacitive elements of the circuit. To reduce resonance in LCL filter, damping resistors are needed. The damping resistors are placed in series with capacitors, which can be seen from LCL filter's single-phase presentation from Fig. 3.6. In that figure L_c is the converter side inductance, L_g is the grid side inductance, V_c is the converter voltage, i_c is the converter current, i_g is the grid current, R_d is the damping resistor and C_f is the capacitance. The damping resistances can also be installed in parallel with grid inductors, but then they do not provide as good attenuation for high frequency harmonics as the series installed resistances do [29]. The damping resistors also enhance the stability of the control system, but on the other hand they produce additional energy losses [28].

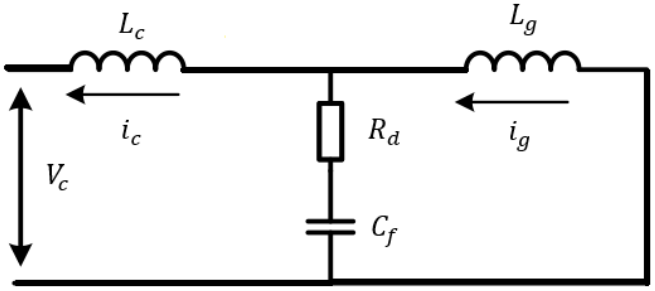

Figure 3.6. *Single-phase equivalent model of the LCL filter.*

The transfer function of the converter voltage V_c and converter current i_c is in the following equation. The problem is to find proper value for damping resistor R_d. It can be found, when the grid current i_g and the converter voltage V_c related to transfer function has a zero at $z = -1/(R_d C_f)$. R_d has to be determined, when the capacitor impedance is at resonant angular velocity ω_{res}. The equations needed for the sizing of the damping resistors are determined [30]:

$$G_c(s) = \frac{i_c(s)}{V_c(s)} = \frac{1}{L_c s} \frac{s^2 + 2\zeta' z_{LC} s + z_{LC}^2}{s^2 + 2\zeta \omega_{res} s + \omega_{res}^2} \tag{3.3}$$

$$\omega_{res}^2 = \frac{L_c + L_g}{L_c} z_{LC}^2 \tag{3.4}$$

$$z_{LC}^2 = \frac{1}{L_g C_f} \tag{3.5}$$

$$\zeta' = \frac{R_d C_f z_{LC}}{2} \tag{3.6}$$

$$\zeta = \frac{R_d C_f \omega_{res}}{2} \tag{3.7}$$

where ‘s’ is a Laplace variable, ζ' and ζ are damping factors. Equations (3.4) and (3.5) are combined together and the result can be used for calculating the resonant angular velocity as:

$$\omega_{res} = \sqrt{\frac{L_c + L_g}{L_c L_g C_f}} = 7607 \ \frac{rad}{s} \tag{3.8}$$

After the resonant angular velocity is determined, the size of the damping resistor at star connection can be calculated in a point, where the transfer function has a zero and it is determined by the following:

$$R_{dY} = \frac{1}{\omega_{res} C_f} = 2.73\ \Omega \tag{3.9}$$

where R_{dY} is the size of damping resistor in star connection. The damping resistors are in delta connected, thus the used damping resistors are calculated by the following:

$$R_{d\Delta} = 3 * R_{dY} = 8.22\ \Omega \tag{3.10}$$

where $R_{d\Delta}$ is the size of damping resistor in delta connection. According to Liserre [31], the size of damping resistor what is needed for this application is 1/3 of filter's capacitive impedance at resonant angular velocity, which is calculated by the following:

$$R_d = \frac{1}{3} * R_{d\Delta} = 2.73\ \Omega \tag{3.11}$$

From the laboratory was found multiple size of 1.5 Ω resistors, which were suitable for our application. Thus, was decided to put two resistors in series, which led to 3 Ω and it was close enough to the calculated value of the damping resistor. From Fig. 3.7(a) can be seen the implemented resistors and from Fig. 3.7(b) how they are mounted on the test bench.

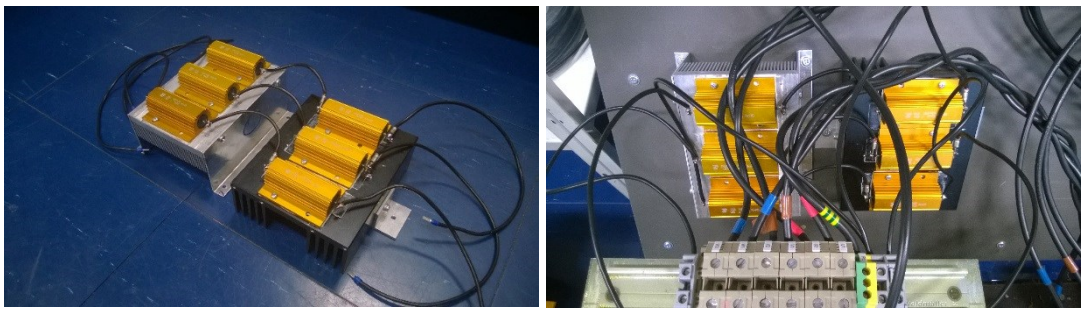

(a) *(b)*

Figure 3.7. *Series connected damping resistors in LCL filter (a) not mounted (b) mounted on the test bench.*

Only one LCL filter requires the damping resistors, because the motor side has Danfoss own control and the damping is already implemented to their software.

3.5 Measurement circuitry

The measurements in the test bench are done by using commercial equipment. Current and voltage measurement sensors were ordered from Imperix, the manufacturer of the Boombox. The measurements of the torque and rotating speed are done by using torque transducer, which was ordered from Datum Electronics.

3.5.1 Current and voltage measurements

Current measurements are done by a sensor, shown in Fig. 3.8(a) and the installed measurements are seen from Fig. 3.10. The current sensor is connected to the Boombox by Ethernet cable, which transmits data transfer and the power supply. The measurements of the current sensors are done in series. The maximum current of the sensor is ±50 A, sensitivity 99 mV/A, typical precision ±0.45 %, the minimum measurement bandwidth 200 kHz and input impedance 2.1 mΩ [32]. The current sensor is based on LEM's current transducer, whose model is LAH 50-P. The current measurement circuit is shown in Fig. 3.8(b).

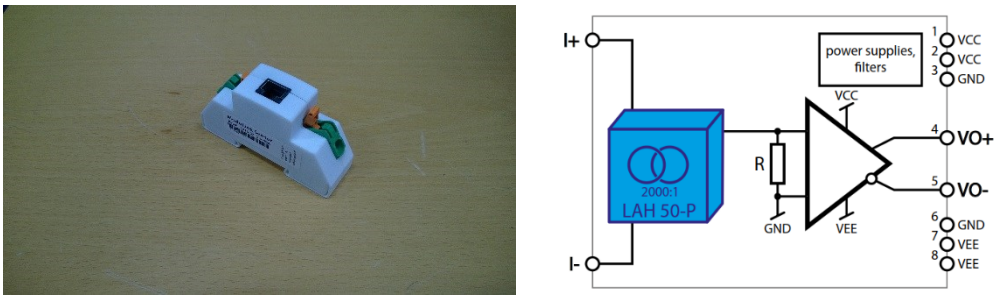

(a) (b)

Figure 3.8. *(a) Current sensor and (b) its measurement circuit [32].*

Voltage measurements are done by a sensor, shown in Fig. 3.9(a). The voltage sensor is connected in the same way as was the current sensor except the measurements of the voltage sensors are done in parallel. The maximum voltage of the sensor is ±800 V, sensitivity 2.46 mV/V, typical precision ±0.15 %, the minimum measurement bandwidth 60 kHz and input impedance 8 MΩ [33]. The voltage measurement circuit is shown in Fig. 3.9(b).

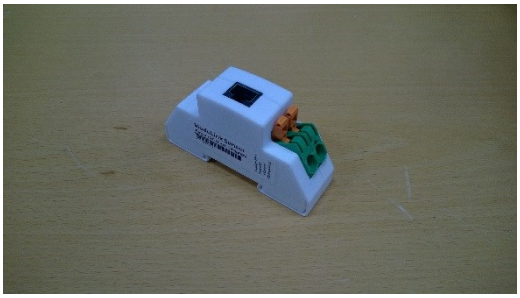

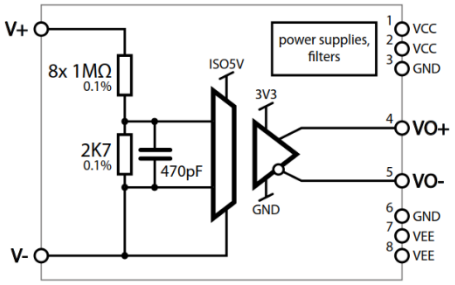

(a) (b)

Figure 3.9. *(a) Voltage sensor and (b) its measurement circuit [33].*

Figure 3.10. *Installed current and voltage sensors.*

In Fig. 3.10 there are overall 14 sensors, which measure grid and generator side currents and voltages. Also the DC-link current and voltage are measured in the generator side.

3.5.2 Torque transducer and incremental encoder

As explained in Chapter 3.2 a torque transducer was installed between the generator and motor. Our transducer was ordered from Datum Electronics, which can be seen from Fig 3.11. There is the transducer without clutches and Datum universal interface (DUI), which is used for monitoring output values. The analog output values, which can be monitored are power, rotating speed, torque and thrust. The transducer's ppr (pulses per revolution) number is 30, which means that it might not be enough for low rotating machines and the measured results might have too much error. Thus, there are incremental encoders inside both machines, which provide 2048 ppr. That amount of pulses per revolution guarantees accurate measurements for low rotating speeds. The rotating speed of the generator and motor have to be same, because they are coupled together via transducer and clutches. There may be some vibrations in coupling, which might cause some angle error between these two machines. Thus, two individual encoders are required for both machines. The

encoders used are from Leine&Linde, the model is XHI 861 and were installed in machines already in the factory. The maximum output frequency of the encoder is 200 kHz, the maximum rotational speed 6000 rpm and the dividing error ±50 °el [34].

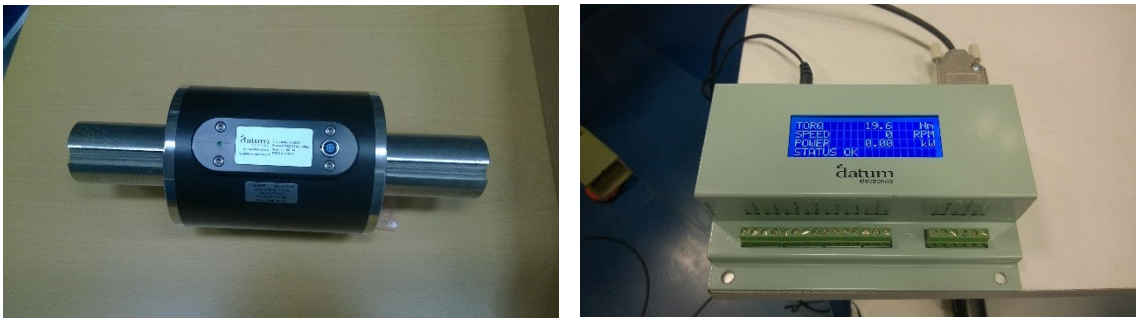

(a) *(b)*

Figure 3.11. *(a) Datum transducer and (b) Datum universal interface.*

The transducer's model is M425, the maximum rotating speed is 6000 rpm and the maximum load is 2000 Nm. DUI provides a graphical display and multiple outputs for an external device. Analog outputs are configurable. All the outputs were set to 4-20 mA, because the current signal is less disturbance than the voltage signal. Therefore, it is possible to connect torque and speed outputs to Boombox via Ethernet cables. DUI can also be connected to the computer and use the graphical user interface, which was provided by the Datum Electronics for monitoring measured values. Also other configurations and PC data logging can be done via computer.

3.6 The complete system

The converters are shown in Fig. 3.12 and the complete test bench is shown in Fig. 3.13. The machines fans are powered by smaller IMs, which are connected to the laboratory's network. The implementation of the self-made control system is not done in this thesis.

Figure 3.12. *The converters and the filters.*

In the Fig. 3.12 the laboratory's supply voltage is connected to the junction box, where are located on/off-device and separators. The converters are divided to generator and motor side, which are then connected to the corresponding LCL filter.

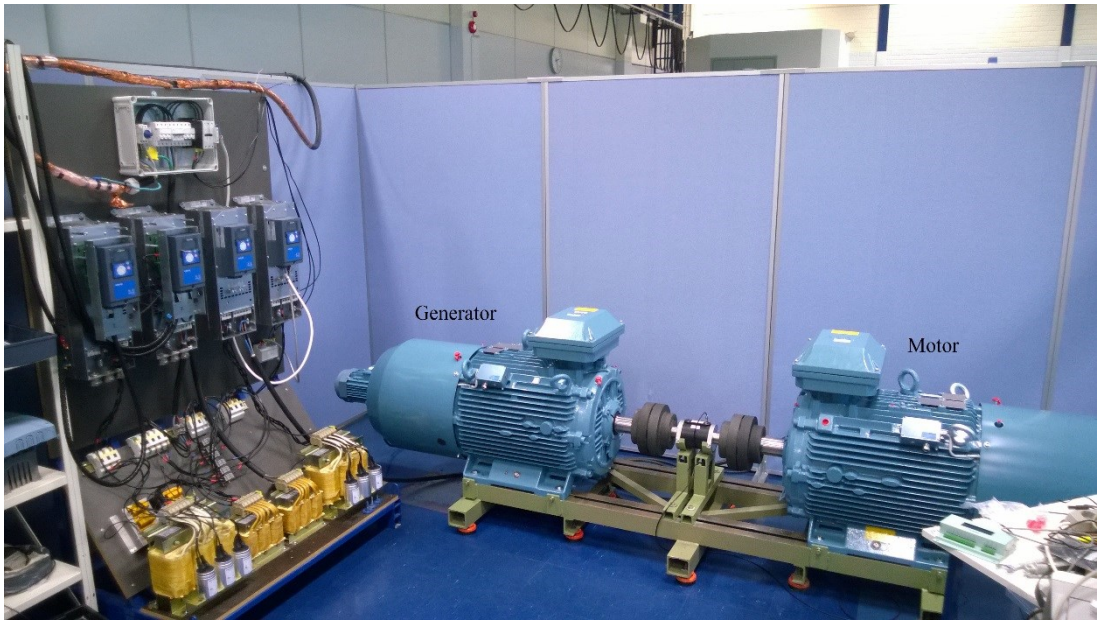

Figure 3.13. *The complete test bench.*

In Fig. 3.13 there is overall picture of the test system. After the machines, converters, filter and junction box were installed, it was possible to check the operation of the test system, which is done in Chapter 4.

4 SIMULATION AND TESTING

The control system of PMSG was created by MATLAB Simulink based on the dynamic equations in Chapter 2.5 and the simulation results are introduced in Chapter 4.1. Chapter 4.2 consists of test results, which were done by using the real motor without load. The main idea was to verify the motor's operation. The measured voltages and currents were drawn into oscilloscope. The torque and the rotating speed were measured by Datum Electronics DUI, which saved the data to USB in Excel file.

4.1 Simulation results

In the Simulink model conventional continuous PI-controllers were used for speed and current control. The Simulink model implementation is shown in Fig. 4.1, which uses the following transfer function:

$$G_c(s) = K_p(1 + \frac{1}{T_i s}) \tag{4.1}$$

where K_p is known as proportional gain and T_i is known as the integration time. There is also implemented an anti-windup-technique in the controller for preventing the saturation. With help of the anti-windup-technique, the controllable error values have less overshoot. The controllers have to be designed to be fast without oscillations. Fig. 4.1 illustrates the Simulink model of the speed controller, but the Simulink model of the current controller is exactly the same. As shown in Table 4.1 the current controller's dynamics are faster than the speed controller's dynamics. The flux weakening control in the current controllers require limits for voltages.

Table 4.1. *PI-parameters for speed and current controllers.*

	Speed controller	Current controller
K_p	0.5 Nm/rpm	10 Nm
T_i	0.5 s	0.005 s

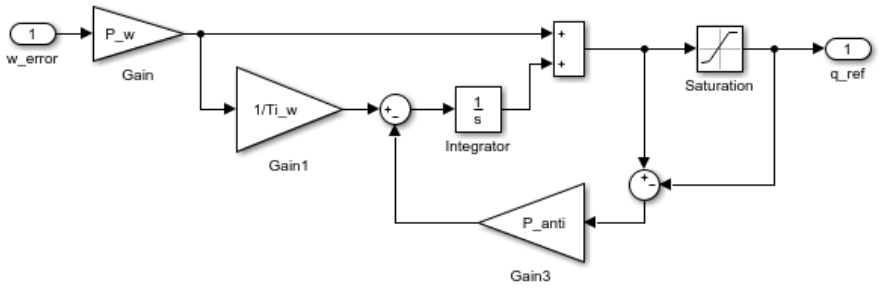

Figure 4.1. *The Simulink model of the PI-controller.*

The created Simulink models of the controls system are presented in Appendix A. In Fig. 4.2 – Fig. 4.6 are simulated wind speed, rotational speed, torque and currents during the changes. The relation between the wind speed, torque and rotating speed require a MPPT-algorithm, which is not developed here. Thus, the simulated reference values are based on the equations (2.16) and (2.17), where the length of the blade is assumed 5.2 m, λ is 6 and c_p is 0.2. In Fig. 4.2 is the wind speed reference, where the first wind speed is 3 m/s at the time of 0.2 s. Then it changes to 5 m/s at the time of 2 s, and last the final wind speed value is 7 m/s, which happens at the time of 4 s.

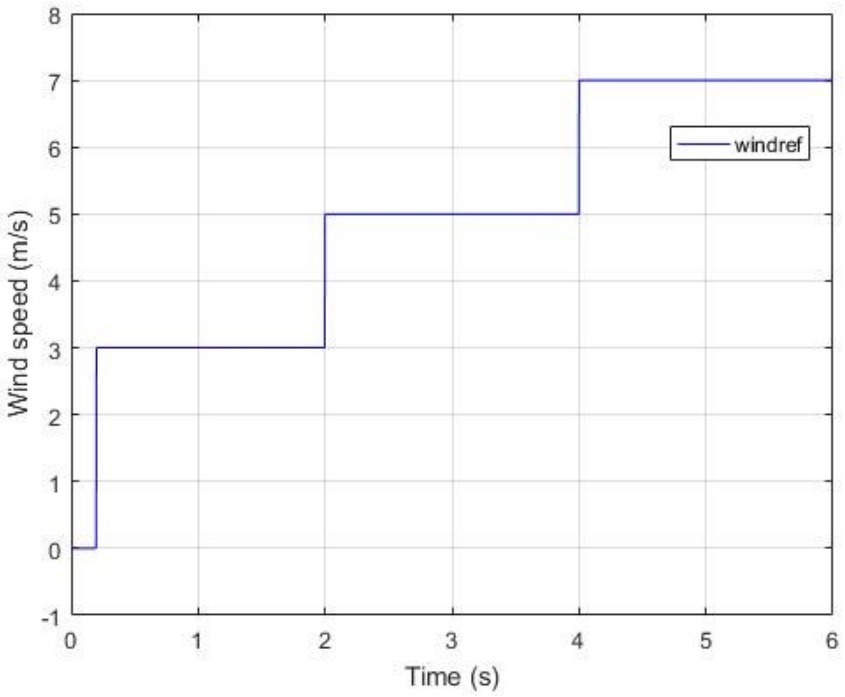

Figure 4.2. *Reference wind speed model.*

Wind speed values in Fig. 4.2 produce specific rotation speed and torque, which can be seen from Fig. 4.3 and Fig. 4.4. The first step happens at 0.2 s, where the wind speed is 3 m/s, which means that it is equivalent in wind turbine model approximately -33 rpm rotation speed and -160 Nm torque. Negative values are used, because a generator is modelled, not a motor. The same principle is used for steps at 2 s, where the rotation speed is -55 rpm and torque -280 Nm. The last step happens at the time of 4 s, where the rotation speed is -77 rpm and torque -450 Nm.

In Fig. 4.3 rotating speed takes only 0.2 s to reach the first step value -33 rpm, because the amount of torque low. When the speed controller reaches the required i_q-current value, the actual speed starts to approach the reference speed, but it also over-shoots slightly. The second and third step are similar except there are no overshoot and it takes 2 s to reach final values in both steps.

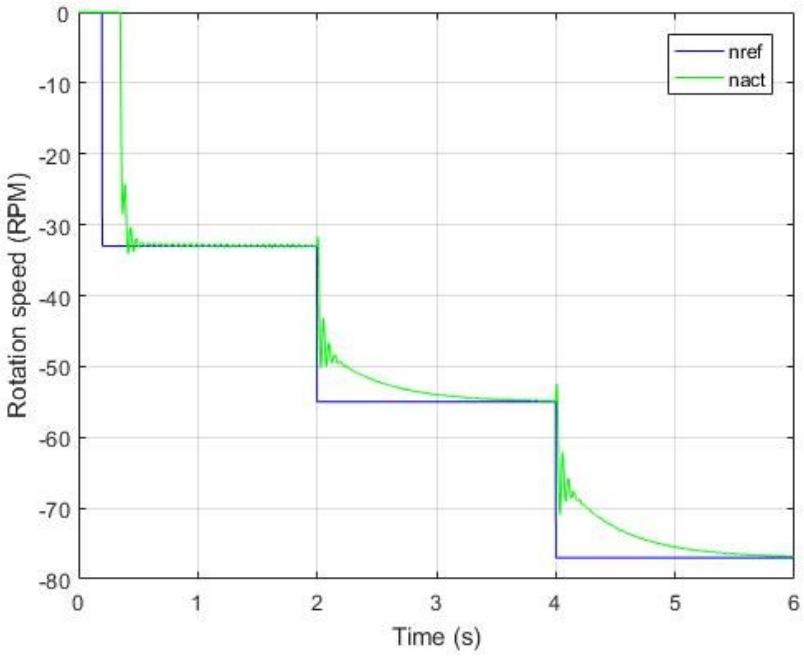

Figure 4.3. *Reference and actual rotating speed.*

In Fig. 4.4 the actual torque follows the reference torque accurately, except those start up transients at the beginning. Those transients are produced, because the rotating speed is zero at the beginning and after the actual rotation speed reaches -33 rpm, the torque reaches the reference value fast.

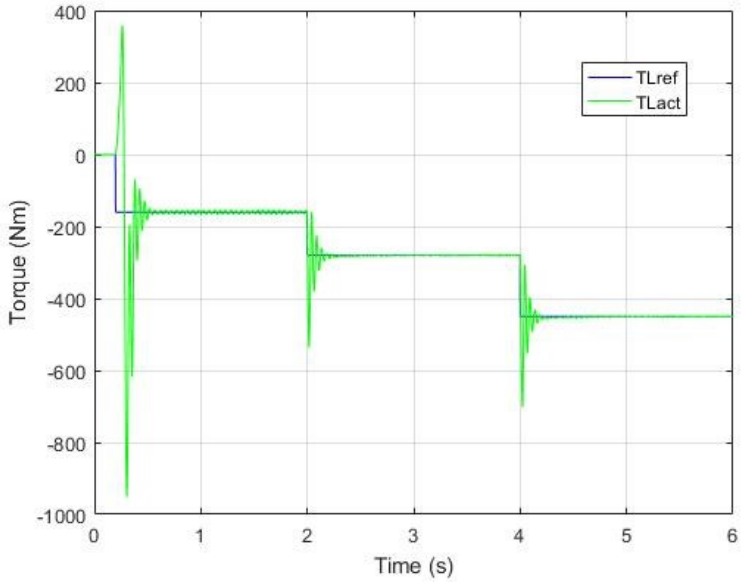

Figure 4.4. *Reference and actual torque.*

In Fig. 4.5 and Fig. 4.6 are shown the dq- and three-phase currents. In Fig. 4.5 after the transients at the beginning the i_d-current step values are 0.8 A, 1.2 A and 1.5 A. The i_q-current step values are -5.5 A, -10 A and -16 A. It is obvious that when more torque and speed are required the stator current component values also increase.

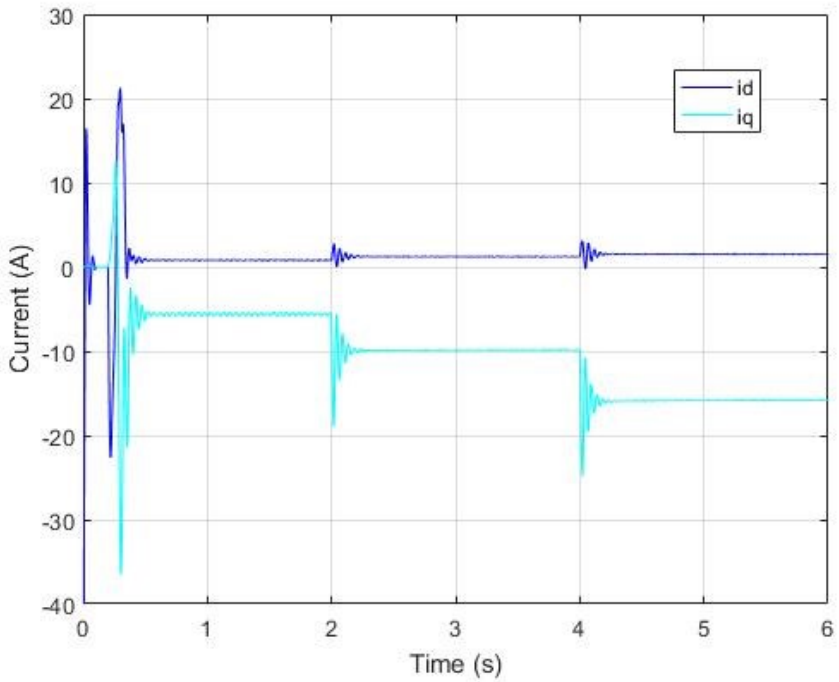

Figure 4.5. *The current components of the generator.*

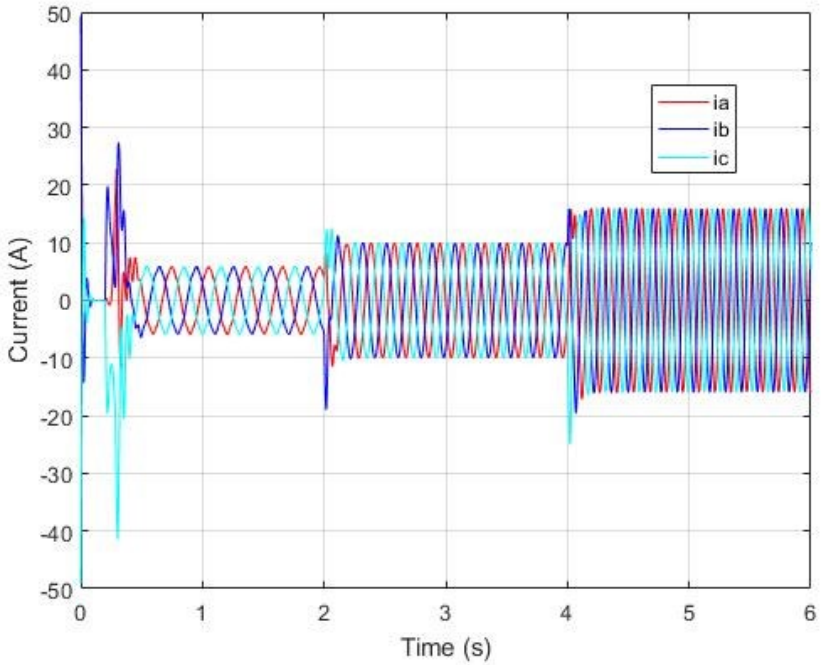

Figure 4.6. *Three-phase currents of the generator.*

In Fig. 4.6 are the three-phase stator currents and their magnitude equals to dq-currents. Three-phase currents are sinusoidal and balanced. The order of the phases is acb, because the angle needed for abc-transformations is negative.

4.2 Test results

The purpose of these tests are verify the operation of the motor and the torque transducer. The tests were done by measuring the rotating speed and torque of the motor by using DUI. The tests were done by without load, because it is unclear how to determine these loads. Setting wrong load might damage the motor, which is not wanted. Therefore no load operation for tests were chosen and the results can be seen from Fig. 4.7 and 4.8. The speed references were 5 Hz and 10 Hz to show proper functioning of the motor and the measurements.

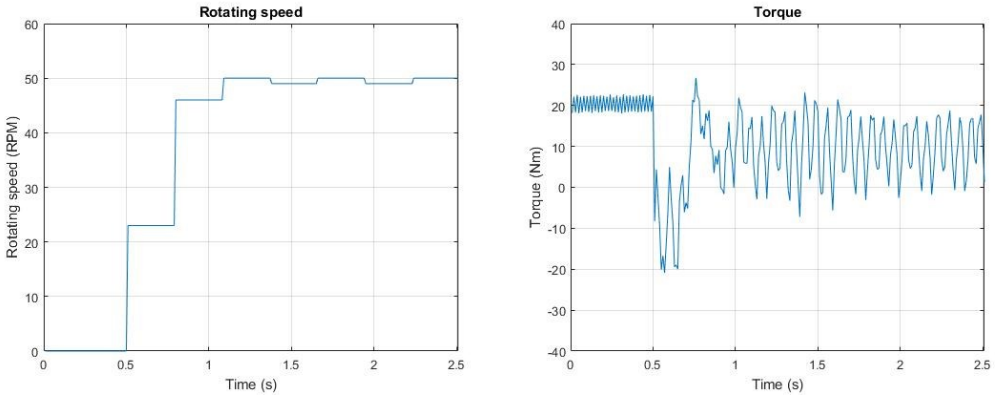

(a) (b)

Figure 4.7. *Rotating speed and torque at 5 Hz.*

In Fig. 4.7(a) is the rotating speed, when the electrical speed reference was 5 Hz. It took only 0.6 s to reach from 0 rpm to 50 rpm. The torque transducer's accuracy is not high enough to collect all the data points during the rise. At the same time in Fig. 4.7(b) the torque drops 10-20 Nm, which is approx. 1% of the rated torque. The initial 20 Nm level is based on the characteristics of the DUI.

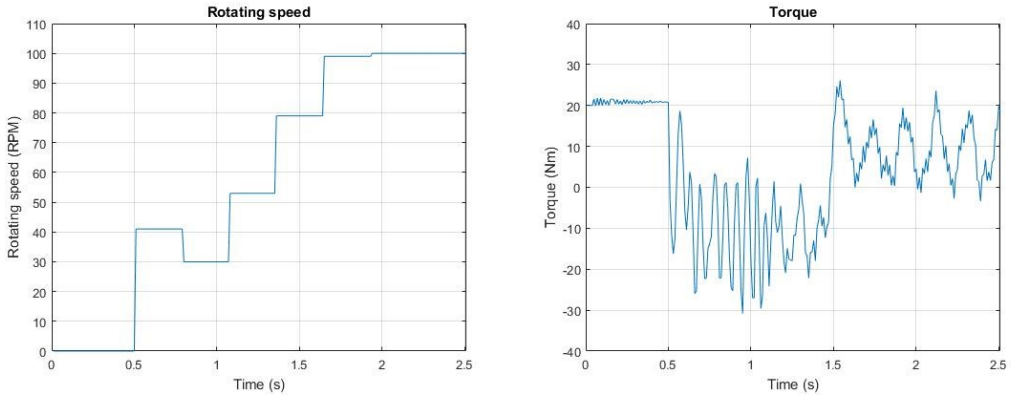

(a) (b)

Figure 4.8. *Rotating speed and torque at 10 Hz.*

In Fig. 4.8(a) is the rotating speed, when the input speed reference was 10 Hz. It took 1.1 s to reach from 0 rpm to 100 rpm. The rise took longer than in 5 Hz case as assumed and now the error in accuracy is multiplied, because at the time of 1 s, the measured acceleration goes negative direction. In Fig. 4.8(b) the torque drops 20-30 Nm, which is approx. 2% of the rated torque.

Voltages and currents were measured at the same time as the torque and the rotating speed. The current measurements were done by using Elditest's current probes. The probes were connected to the motor's cables and an oscilloscope was used to read the measured currents. In Fig. 4.9(a) - 4.11(a) are the motor currents in each phase at reference speed of 5 Hz. In Fig. 4.9(b) – 4.11(b) are the same currents, but at reference speed of 10 Hz.

All the currents magnitudes in Fig. 4.9(a) – 4.11(a) are equally high and the only difference is the phase. The peak value is 5.8 A, which refers to 4.1 A RMS value. The peak value in the Fig. 4.9(b) – 4.11(b) is a little higher, when using reference speed of 10 Hz, but only 7 A, which refers to 5 A RMS value. This means that the current grows only slightly compared to 5 Hz, even though the reference speed was doubled.

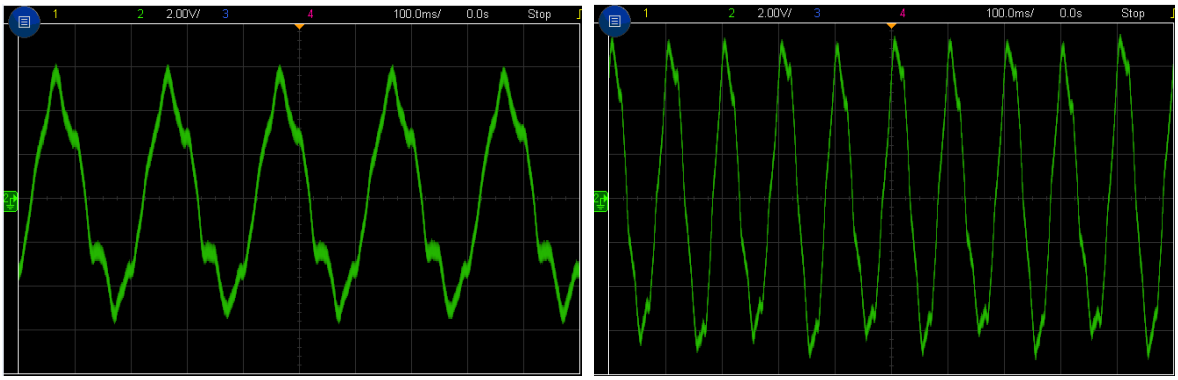

(a) (b)

Figure 4.9. *Measured current at phase a (a) 5 Hz and (b) 10 Hz.*

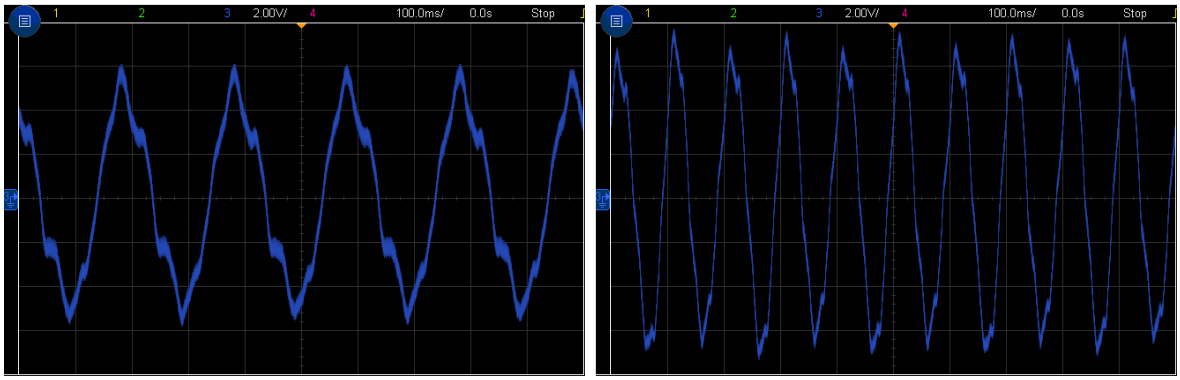

(a) (b)

Figure 4.10. *Measured current at phase b (a) 5 Hz and (b) 10 Hz.*

(a) (b)

Figure 4.11. *Measured current at phase c (a) 5 Hz and (b) 10 Hz.*

The voltages between phases a and b were also measured in the motor and grid side. The measurements were done by using Tektronix high voltage differential probe and reading the data from an oscilloscope. The motor side measurements between phase a and b can be seen from Fig. 4.12. The grid side voltages can be seen from Fig. 4.13.

In Fig. 4.12(a) are the motor voltages between phase a and b at reference speed of 5 Hz. These voltages are not filtered by any means. The voltage is modulated by the PWM, thus it looks like a sawtooth wave. The peak value is near 210 V, thus the RMS value should be 150 V. In the Fig. 4.12(b) is the voltage at rotating speed of 10 Hz. The peak value is 400 V, which means that the RMS value is 280 V. Therefore the current did not grow so much at 10 Hz, because the voltage did.

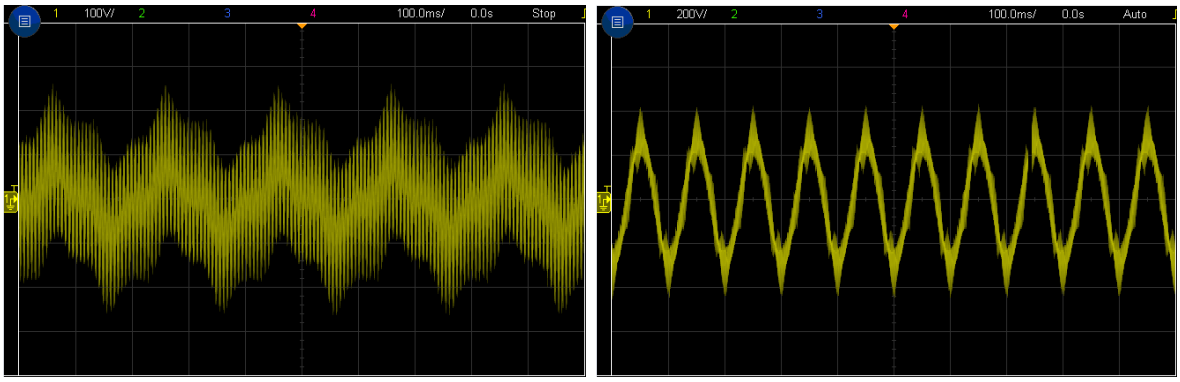

(a) (b)

Figure 4.12. *Measured voltage from motor between phase a and b. Measured at the rotating speeds (a) 5 Hz and (b) 10 Hz.*

Last measurements from the grid voltages are in Fig. 4.13 between phase a and b. The rotating speed does not have any significant influence to the grid voltage.

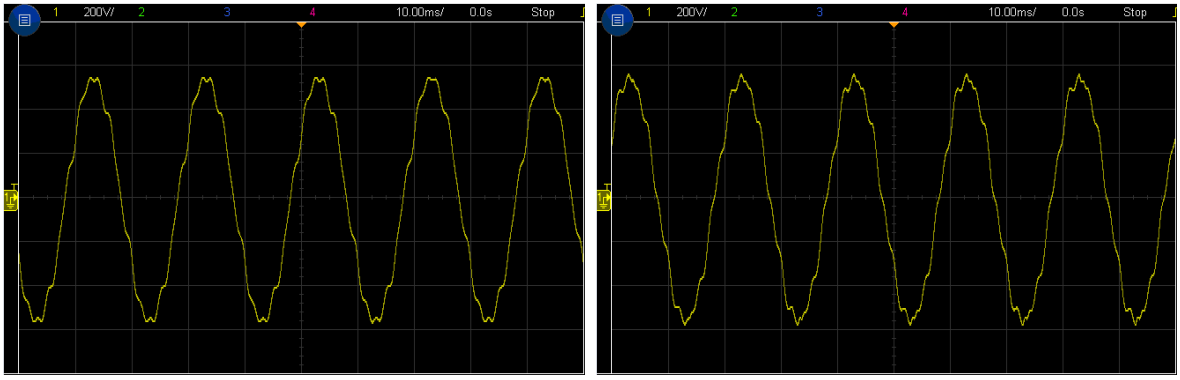

(a) (b)

Figure 4.13. *Measured voltage from grid between phase a and b. Measured at the rotating speeds (a) 5 Hz and (b) 10 Hz.*

There is not much difference between Fig. 4.13(a) and 4.13(b). The peak magnitude in both is 560 V and only a small deviation on the tip of the voltage.

5 CONCLUSION

The amount of energy produced by wind turbines has been increased exponentially during the last years and the trend shows to continue globally. The produced power cannot be controlled as the conventional power generation e.g. water power and the power generated by the fossil fuels. This leads to research questions related to stability of the power grid. How the stability between load and consumed power can be kept? How the wind turbines should operate during the grid faults to support the grid instead of leading to increasing number of problems. To find out answer to these problems, the new wind turbine laboratory has been built.

The purpose of this thesis was to implement a wind power emulating test bench in the laboratory of power electronics. In the test bench was used PMSMs and after it is finished, it will be used for research, where the main focus is on studying the dynamics of the control system. Another research purpose is to model the stator windings numerically based on the measurements windings, which were installed inside the machines.

At the beginning the idea was to build a test bench, where the wind turbine is emulated by a generator and the wind speed is emulated by a motor. The machines would be controlled by the frequency converters, which would have manufacturer's own control in the motor side and our self-made control in the generator side.

The target of the work was to create the dynamic model of IPMSG and create the vector control for the generator in synchronous reference frame in MATLAB Simulink. The vector control required also tuning the PI-controllers. The operation of the control system was proofed by simulations.

The motor and the generator shaft power were 17 kW. After they arrived, they were installed on a base, which was found from laboratory and with small modifications both the generator and the motor fit on the base. Between them was put a torque transducer from Datum Electronics, which can measure torque and rotating speed. It was set between machines by flexible claw clutches. The transducer had to install carefully, because it was very important that the transducer was aligned with the machines.

After the converters came from Danfoss, they were installed in the wall, which was set next to the bench, where the machines were. The converters had diode- and IGBT-bridges and the diode-bridges were then bypassed by connecting the DC-links together in the motor and generator side. This allowed bidirectional power flow. The LCL filters were installed under the converters and the capacitors in the LCL filters required damping resistors in series in the generator side, which were then constructed and installed above the generator side filter.

After the main parts of the test bench were ready, they required also a junction box for the separators where all the right cables were connected. The measurement sensors came from Imperix, which were then installed. In the end were performed step tests to the motor without load to verify its operation and the rotating speed and the torque

were measured by DUI. At the same time the voltages and the currents were measured during the tests by probes, which were then recorded and documented.

Due the schedule reasons, there was no time to complete everything what was planned at the beginning. The space between the machines where the transducer is, requires plastic shields for anybody who uses the bench, will not touch there during its operation. Same thing for filters, because during their operation there are voltages on. The small induction motors in the PMSMs, which rotate the fans of the machines, get their electricity from laboratory's electric network, which was a temporarily solution. Thus, another junction box has to be implemented in the wall, where the small IMs get their electricity. The last thing is to connect the Boombox in the test bench and fasten all the measurement cables from sensors to Boombox. It also requires building a Boombox Simulink model, which allows the use of those measurements.

After this part of the complete system is finished, can be said that the motor worked as expected in the tests. The measurement sensors were modularity and they had a simple structure, therefore it is easy to add more those sensors in the test bench, if needed. The created Simulink model offers a good help for creating the Boombox related Simulink model, where the inputs and outputs of the software part of the Boombox are implemented. The test bench will be used mainly for research purposes, but with some effort it can be developed a wind power related motor lab for students.

REFERENCES

[1] Tietoa ilmastonmuutoksesta. CO2-raportti. [cited 7.6.2017]. Available: http://www.co2-raportti.fi/?page=ilmastonmuutos.

[2] The Paris Agreement. United Nations Framework Convention on Climate Change. [cited 7.6.2017]. Available: http://unfccc.int/paris_agreement/items/9485.php.

[3] Tietoa tuulivoimasta. Suomen Tuulivoimayhdistys. [cited 7.6.2017]. Available: http://www.tuulivoimayhdistys.fi/tietoa-tuulivoimasta/tietoa-tuulivoimasta/miksi-tuulivoimaa.

[4] Corbetta, G., Mbistrova, A., Ho, A. Wind in power 2015 European statistics. 2016. The European Wind Power Association. 14 p.

[5] Bilgin, B., Sathyan, A. Chapter 5. Fundamentals of Electric Machines. In: Emadi, A. Advanced Electric Drive Vehicles. 2014, CRC Press. pp. 107-186.

[6] Kazerooni, M., Hamidifar, S., Kar, N. Analytical modelling and parametric sensitivity analysis for the PMSM steady-state performance prediction. IET Electric Power Applications, vol. 7, 2013, pp. 586-596.

[7] Wu, Z., Dou, X., Chu, J., Hu, M. Operation and Control of a Direct-Driven PMSG-Based Wind Turbine System with an Auxiliary Parallel Grid-Side Converter. July 2013, MDPI, pp. 3405-3421.

[8] Mäkinen, A.S., Messo, T., Tuusa, H. Power hardware in-the-loop laboratory test environment for small scale wind turbine prototype. Power Electronics and Applications (EPE'14-ECCE Europe), 2014 16th European Conference, August 2014, IEEE, 10 p.

[9] Bastman, J. TEL-1330 Sähkökoneet. 2011, Tampere University of Technology. 189 p.

[10] Hughes, A., Drury, B. Electric Motors and Drives. Fourth Edition. 2013. 436 p.

[11] Rahman, M.A. Electrical Engineering Handbook, Power Electronics and Motor Drives, Chapter 5. Permanent Magnet Machines. 2011, CRC Press, 10 p.

[12] Haikola, M. ABB Review Pathways to innovation. Helsinki, 2009. 6 p.

[13] Kennel, R. Power Electronics Exercise: Space Vector. 2012, München University of Technology. 16 p.

[14] Mohan, N. Advanced Electric Drives: Analysis, Control, and Modeling Using MATLAB/Simulink. 2014, John Wiley & Sons. 208 p.

[15] Ohm, D.Y. Dynamic Model of PM Synchronous Motors. Drivetech, Inc., Blacksburg, Virginia. 10 p.

[16] Mäkinen, A. Investigations and Real Time Testing of Variable Speed Wind Turbine Control during Grid Faults. 2017, Tampere University of Technology. 112 p.

[17] Rekola, J. Modeling and control of electric drives lecture 6: synchronous machine dynamic model. 2015, Tampere University of Technology. 60 p.

[18] Hau, E. Physical Principles of Wind Energy Conversion. 3rd edition. 2013, Springer-Verlag Berlin Heidelberg. 879 p.

[19] Barisa, T., Sumina, D., Kutija, M. Control of Generator- and Grid Side Converter for the Interior Permanent Magnet Synchronous Generator. 4th International Conference on Renewable Energy Research and Applications. November 2015, pp. 1015-1020.

[20] Raju, N.I., Islam, S., Uddin, A. Sinusoidal PWM Signal Generation Technique for Three Phase Voltage Source Inverter with Analog Circuit & Simulation of PWM Inverter for Standalone Load & Micro-grid System. International Journal of Renewable Energy Research, vol. 3, no. 3, pp. 647-658.

[21] Gole, A.M. 24.437 Power Electronics, Sinusoidal Pulse Width Modulation, Course notes. 2000, University of Manitoba. 8 p.

[22] Knapczyk, M., Pienkowski, K. Analysis of Pulse Width Modulation Techniques for AC/DC Line-side Converters, Scientific Papers of the Institute of Electrical Machines, Drives and Metrology of the Wroclaw University of Technology, no. 59, study material, no. 26, 2006. 16 p.

[23] Shi, Y., Sun, K., Huang, L., Li, Y. Control Strategy of High Performance IPMSM Drive in Wide Speed Range. 2011, IEEE, pp. 1783-1788.

[24] Uddin, M.N., Rahman, M.A. High Speed Control of IPMSM Drives Using Improved Fuzzy Logic Algorithms. IEEE Transactions on Industrial Electronics, vol. 54, no. 1, February 2007, pp. 190-199.

[25] Fouad, G. AC Electric motor controls. 2013, John Wiley & Sons. 578 p.

[26] Kronberg, A. Design and Simulation of Field Oriented Control and Direct Torque Control for a Permanent Magnet Motor with Positive Saliency. 2015, Uppsala Universitet. 56 p.

[27] Hemminki, P. Vaihtosuuntaajan ohjaus dSPACE:lla : diplomityö. Tampere, 2005. Tampere University of Technology. Department of Electrical Engineering, Power Electronics. 77 p.

[28] Beres, R., Wang, X., Blaabjerg, F., Leth Bak, C., Liserre, M. Improved Passive-Damped LCL Filter to Enchance Stability in Grid Connected Voltage-Source Converters. 23rd International conference on electricity distribution (CIRED), 2015, pp. 1-5.

[29] Renzhong, X., Lie, X., Junjun, Z., Jie, D. Design and Research on the LCL Filter in Three Phase PV Grid-Connected Inverters. International Journal of Computer and Electrical Engineering, vol. 5, no. 3, June 2013, pp. 322-325.

[30] Pena-Alzola, R., Liserre, M., Blaabjerg, F., Sebastian, R., Dannehl, J., Fuchs, F. Analysis of the Passive Damping Losses in LCL-Filter-Based Grid Converters. IEEE Transactions on Power Electronics, vol. 28, no. 6, June 2013, pp. 2642-2646.

[31] Liserre, M., Blaabjerg, F., Hansen, S. Design and Control of an LCL-Filter-Based Three-Phase Active Rectifier. IEEE Transactions on Industry Applications, vol. 41, no. 5, September 2005, pp. 1281-1291.

[32] 50 A Din Rail-mountable Current Sensors. imperix SA. 2016, Switzerland. 2 p.

[33] 800 V Din Rail-mountable Voltage Sensors. imperix SA. 2016, Switzerland. 2 p.

[34] Encoder model XHI 861, X-heavy duty Hollow shaft encoder, Incremental. Leine&Linde. 2017. 2 p.

[35] Pokkinen, O. Tuulivoimakäytön laboratoriotestausjärjestelmä: diplomityö. Tampere, 2010. Tampere University of Technology. Department of Electrical Energy Engineering. 78 p.

APPENDIX A

In Appendix A is collected all the created MATLAB Simulink models together. The models are based on the dynamic equations of the PMSM as determined in equations (2.8) – (2.15). The main blocks are presented first, then continuing to sub-blocks. The used parameters in the Simulink models are based on Table 3.1 parameters. The estimated mathematical constants in the Simulink model are for inertia 2.2 kgm^2 and for friction coefficient 0.02 Nm/(rad/s). The used switching frequency in the PWM modulator can vary between 0-20 kHz, but 10 kHz frequency was chosen. DC-voltage is set to 560 V as it is, when the diode rectifier is used. All the main models of the PMSM are in Fig. A.1-A.13. The models in Fig. A.14-A.16 were used in the field weakening control, where were required limits for preventing saturation. The limits are presented in [25].

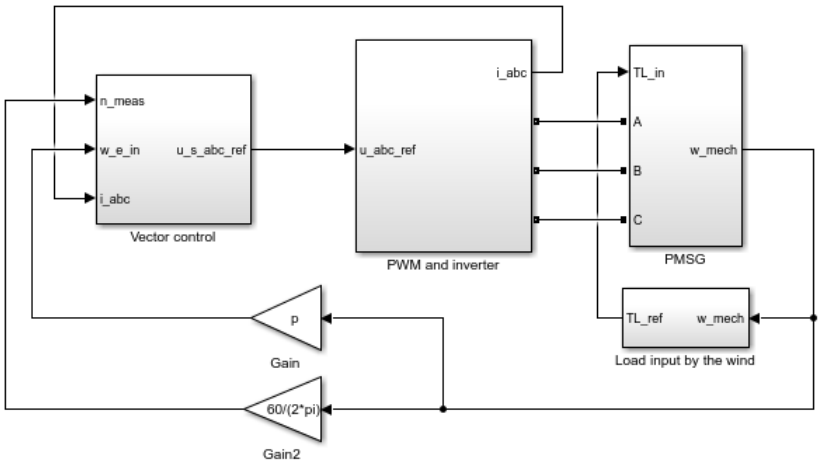

Figure A.1. *The overall model of control systems and PMSG.*

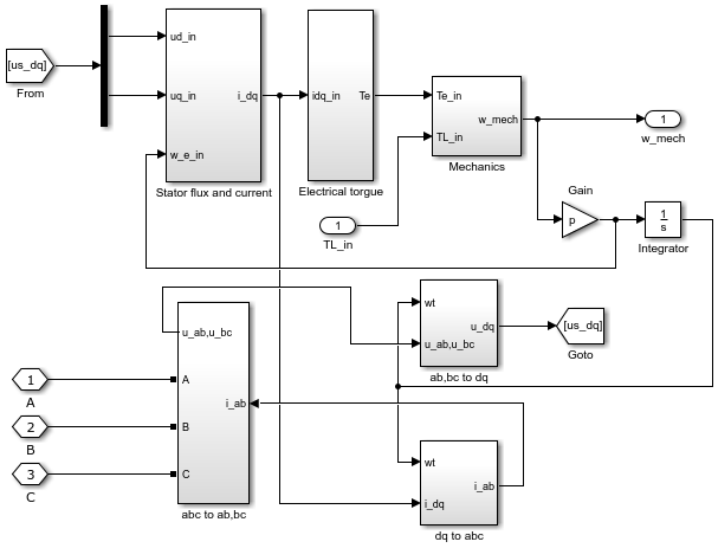

Figure A.2. *The Simulink model of interior PMSG.*

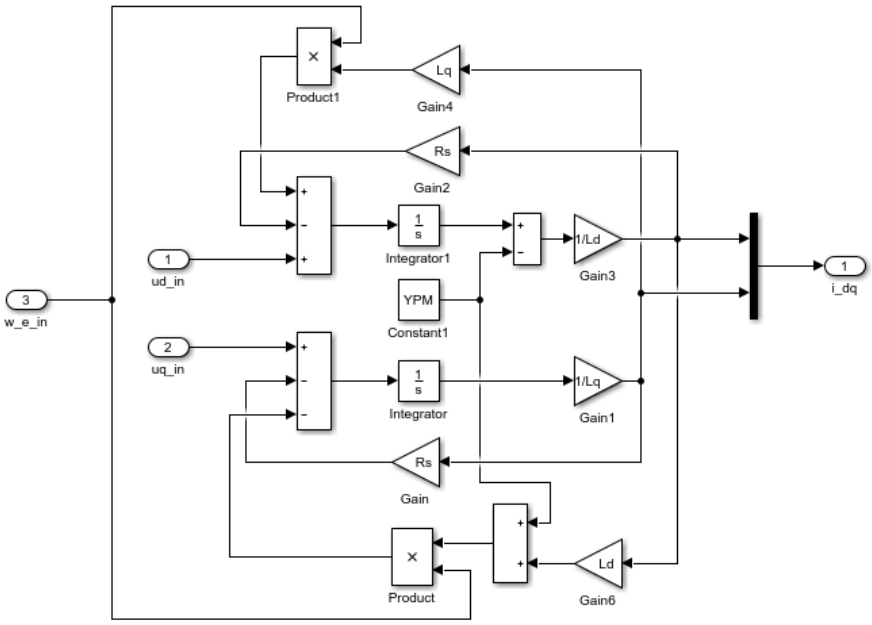

Figure A.3. *Stator flux and current.*

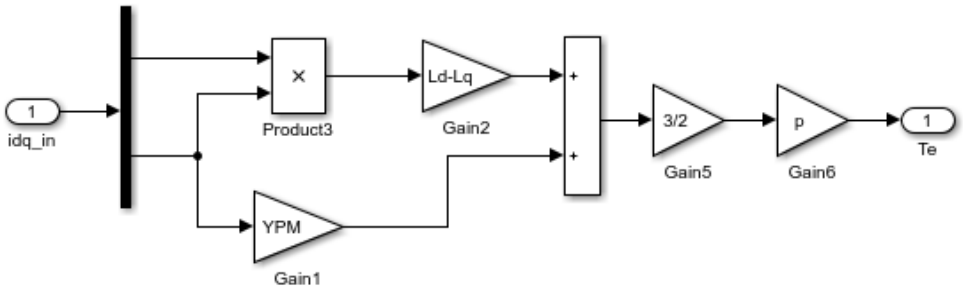

Figure A.4. *Electrical torque.*

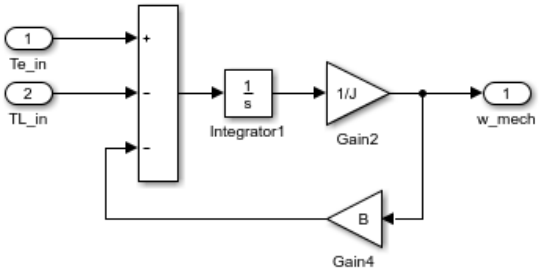

Figure A.5. *Mechanics.*

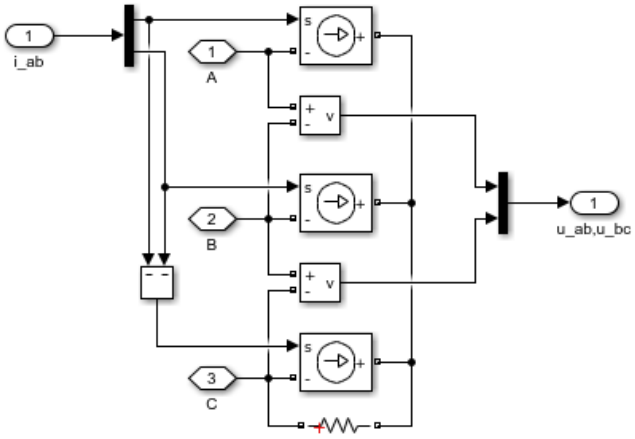

Figure A.6. *Line-to-line voltages from measured phase voltages and currents [modified 35].*

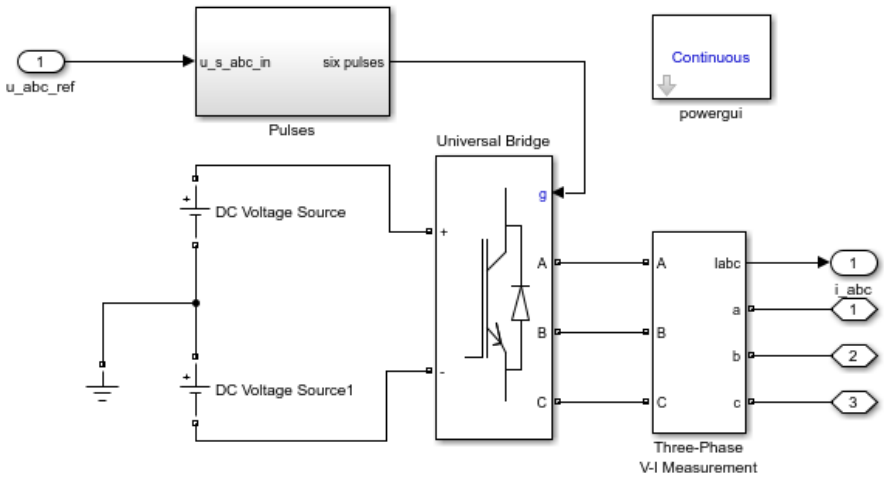

Figure A.7. *The Simulink model of the inverter, PWM and assumed ideal DC-voltage sources.*

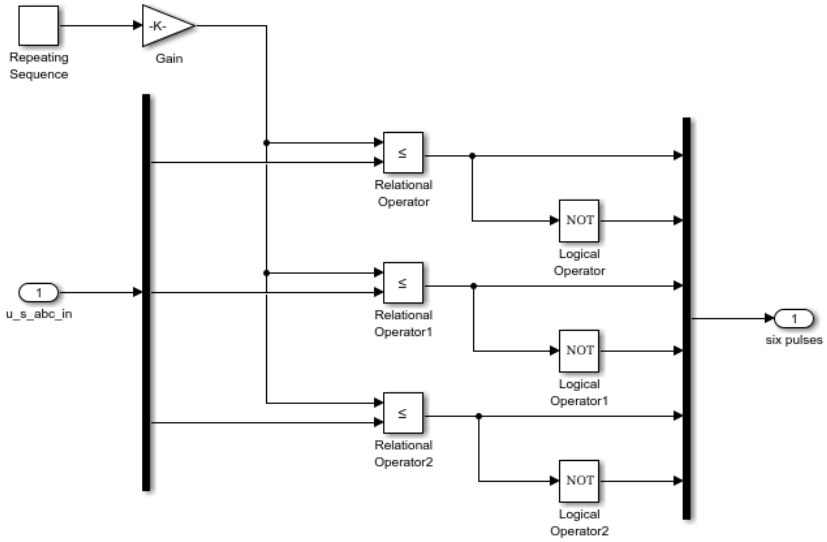

Figure A.8. *Pulse width modulation (PWM) in Simulink.*

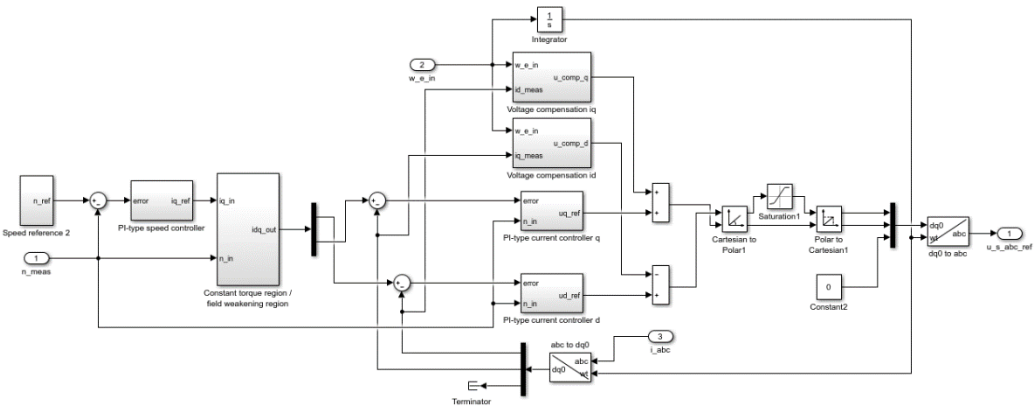

Figure A.9. *Vector control system.*

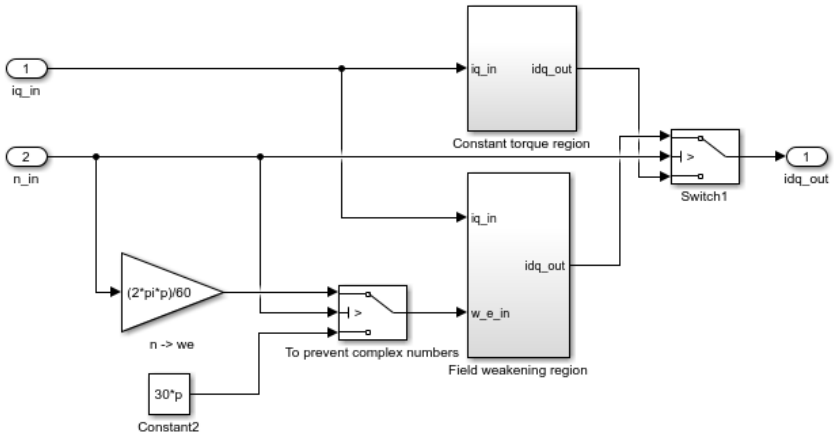

Figure A.10. *The current reference calculation based on the machine speed.*

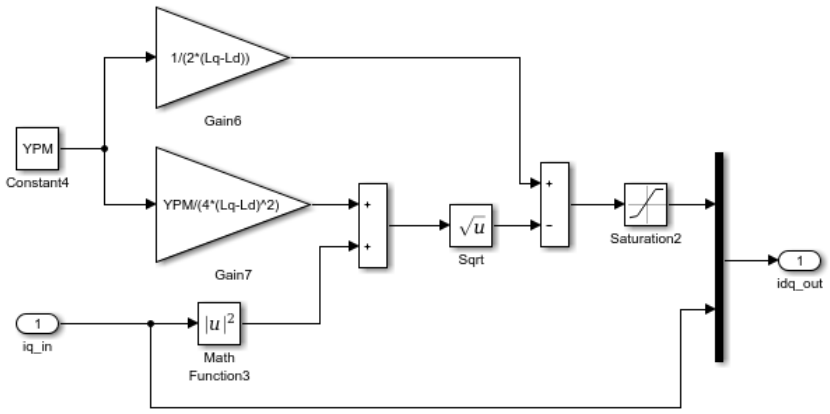

Figure A.11. *Constant torque region.*

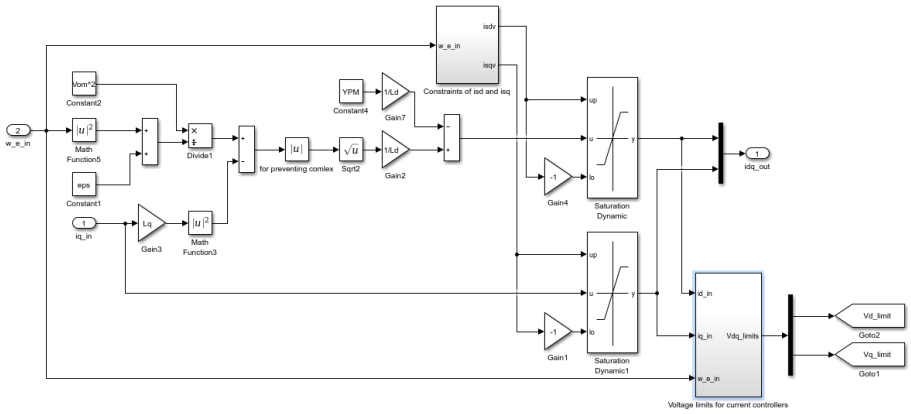

Figure A.12. *Field weakening region where the current constraints and voltage limits calculations are based on the machine speed.*

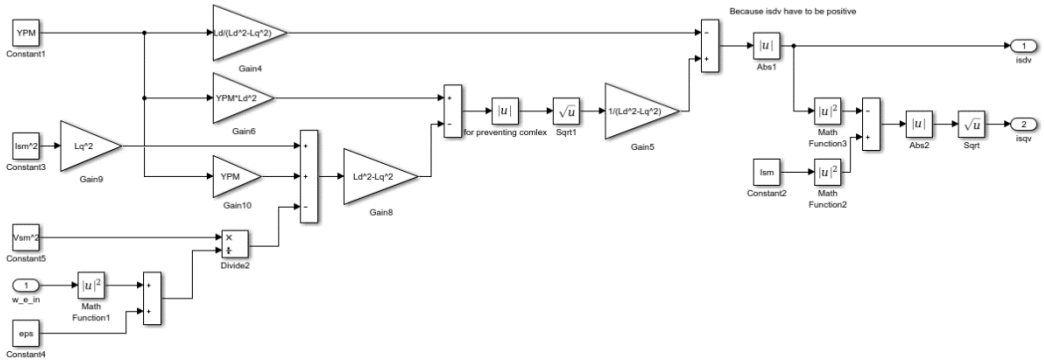

Figure A.13. *Constraints of isd and isq in field weakening region.*

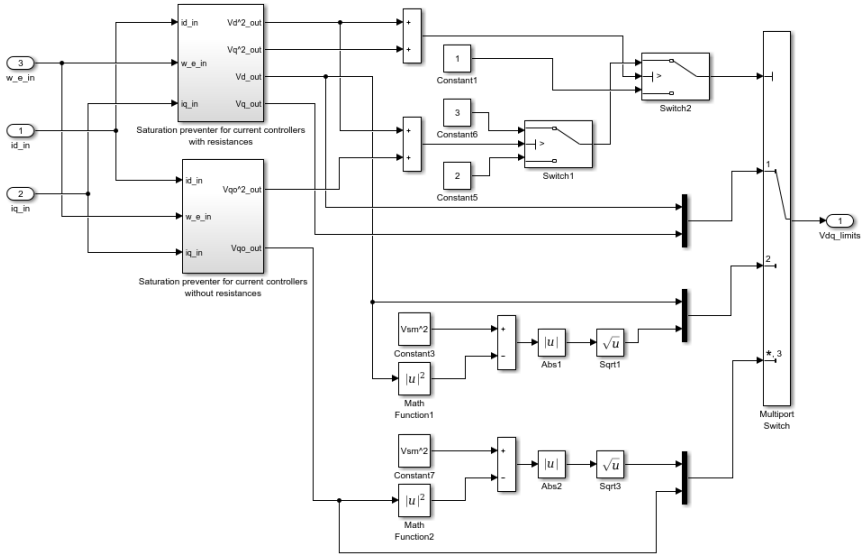

Figure A.14. *Voltage limits for current controllers in field weakening region [25].*

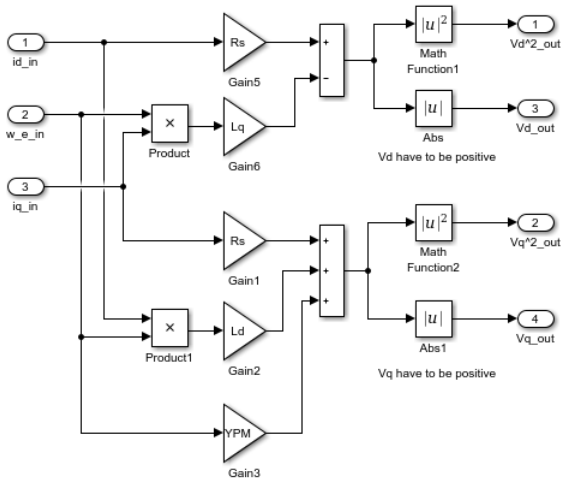

Figure A.15. *Saturation preventer for current controllers with resistances, which are needed for voltage limits calculations [25].*

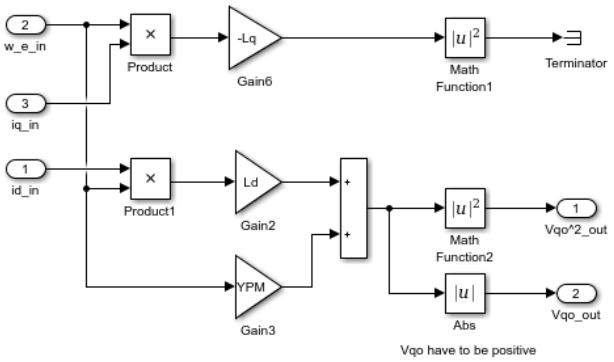

Figure A.16. *Saturation preventer for current controllers without resistances, which are needed for voltage limits calculations [25].*